18A

PNL-3203
UC-90b

FY-1979 Progress Report Hydrotransport Plugging Study

L. L. Eyler
N. J. Lombardo

January 1980

Prepared for the U.S. Department of Energy
under Contract EY-76-C-06-1830

Pacific Northwest Laboratory
Operated for the U.S. Department of Energy
by Battelle Memorial Institute

Battelle

PNL-3203

NOTICE

PACIFIC NORTHWEST LABORATORY
operated by
BATTELLE
for the
UNITED STATES DEPARTMENT OF ENERGY
Under Contract EY-76-C-06-1830

Printed in the United States of America
Available from
National Technical Information Service
United States Department of Commerce
5285 Port Royal Road
Springfield, Virginia 22151

Price: Printed Copy $____*; Microfiche $3.00

*Pages	NTIS Selling Price
001-025	$4.00
026-050	$4.50
051-075	$5.25
076-100	$6.00
101-125	$6.50
126-150	$7.25
151-175	$8.00
176-200	$9.00
201-225	$9.25
226-250	$9.50
251-275	$10.75
276-300	$11.00

PNL-3203
UC-90b

FY-1979 PROGRESS REPORT

HYDROTRANSPORT PLUGGING STUDY

L. L. Eyler
N. J. Lombardo

January 1980

Prepared for
the U.S. Department of Energy
under Contract EY-76-C-06-1830

Pacific Northwest Laboratory
Richland, Washington 99352

ACKNOWLEDGMENTS

The authors would like to acknowledge the assistance of J. W. Shupe, J. D. Smith, and K. D. Hinkle during various phases of the experimental work conducted in this study. The technical support and encouragement of A. J. Miscoe and R. C. Wang (DOE, Pittsburgh Mining Technology Center) have provided invaluable guidance to this study.

Technical discussions were held with the following individuals:

D. J. Judge, Queens University

D. T. Kao, University of Kentucky

R. R. Faddick, Colorado School of Mines

G. A. Pouska, Colorado School of Mines Research Institute

The contribution of their time is appreciated.

Funding support for this study came from the U.S. Department of Energy, Division of Fossil Fuel Extraction.

The assistance of A. J. Currie in report preparation and technical editing must also be acknowledged.

SUMMARY

The objective of the Hydrotransport Plugging Study is to investigate phenomena associated with predicting the onset and occurrence of plugging in pipeline transport of coal. This study addresses large particle transport plugging phenomena that may be encountered in run-of-mine operations. The project is being conducted in four tasks: review and analysis of current capabilities and available data, analytical modeling, experimental investigations, and unplugging and static start-up. This report documents work completed in FY-1979 as well as work currently in progress. Summaries of progress on individual tasks follow.

TASK 1: REVIEW

A review of currently available prediction methods was completed. Applicability of the methods to large particle hydrotransport and the prediction of plugging was evaluated. During this review it was determined that available models were inadequate, either because they are empirical and tuned to a given solid or because they are simplified analytical models incapable of accounting for a wide range of parameters. Complicated regression curve fit models lacking a physical basis cannot be extrapolated with confidence.

One problem encountered continuously in hydrotransport literature was the absence of a consistent set of symbols for nomenclature. This is not an insurmountable problem, although it can lead to confusion in model comparison. Another problem was the definition of "plugging." Physically, it seems reasonable to assume a plugged situation occurs when no solids are being delivered by the pipeline. However, several definitions and related criteria are available. These criteria are concerned with prediction of a point of minimum pressure drop or the point where solids begin to deposit in the pipe. Although these conditions correspond to a situation in which delivered solids begin to decrease, they are not necessarily congruent with a plugged situation in a physical sense.

Several specific conclusions were reached based on information obtained in this task. These included:

- Recent developments in mechanistic modeling, describing flow conditions at the limit of stationary deposition, provide the best basis for prediction and extrapolation of large particle flow.
- Certain modeled phenomena require further analytical and experimental investigation to improve confidence levels.
- Experimental work needs to be performed to support modeling and to provide an adequate data base for comparison purposes.
- No available model permits a separate treatment of solids mixtures such as coal and rock.

TASK 2: ANALYTICAL MODELING

Analytical modeling efforts are currently in progress. Based on the results of Task 1, a mechanistic model developed for predicting the point of stationary deposition is being extended and modified. In addition, modeling aspects of throughbed flow, interfacial shear, turbulent suspension, and particle size distribution are to be investigated. Mechanisms of two-solid flow are also being evaluated using the single-solid model as a basis. The goal of this task is to provide a better understanding and basic prediction method applicable to run-of-mine rock and coal mixtures.

TASK 3: EXPERIMENTAL INVESTIGATIONS

The objective of the experimental work being conducted in support of the project is to provide a data base upon which better model predictions can be based. In particular, two experiments designed to isolate particular phenomena are to be conducted. Both are directly related to the formulation of a mechanistic model needed to predict the limit of stationary deposition.

The initial experiment completed in FY-1979 used a tiltable pipe test section to determine the effects of particle size and bed depth on the sliding friction force for submerged coal and rock in a pipe. Sliding friction is one

of the resisting forces that exist during normal, low-flow, bed-load operation of a pipeline. An accurate representation of this force is necessary to support the modeling effort.

The second and ongoing experiment involves investigation of interfacial shear caused by fluid flow through a pipe with a predominantly stationary bed-load of solids. Interfacial shear is included as a driving force in this flow regime and is currently modeled assuming a friction factor proportional to an equivalent sand grain roughness. This experiment is intended to either verify the equivalent roughness assumption for large particles or provide a data base for developing an alternative approach.

TASK 4: UNPLUGGING AND STATIC START-UP

This task is in the planning stage and is scheduled to be performed in FY-1981.

CONTENTS

FIGURES

TABLE

NOMENCLATURE

Symbol	Description
a	Fraction of flow area above solids bed
A_p	Pipe cross-sectional area
A_{plate}	Surface area of a plate
A_{wall}	Surface area of a pipe wall
b_1, b_2	Two-solid model bed area fractions
C_b	Volumetric concentration of loose-packed bed
C_c	Volumetric concentration of bed contact load
C_d	Delivered volumetric concentration
C_D	Drag coefficient
C_i	*In situ* volumetric concentration
C_r	Relative volumetric concentration, $C_r \equiv C_d/C_b$
C_{Rh}	Relative volumetric concentration of suspended solids
C_{s1}, C_{s2}	Individual solids concentration
C_w	Weight fraction
d	Characteristic particle size
$\bar{d}$	Characteristic weighted average particle size
d_{50}	Characteristic particle size corresponding to sieve opening passing 50% of solids
D	Pipe diameter
D_h	Hydraulic diameter
f	Friction factor
f_b	Base friction factor

Symbol	Description
f_{bed}	Friction factor for a steel test section with a solids bed present
f_i	Friction factor due to surface roughness of fixed particles on a plate
$f_{i,eff}$	Effective interfacial friction factor $f_{i,eff} = f_{bed} - f_{plate}$
f_m	Mixture friction factor
f_o	Clear fluid friction factor
f_{plate}	Friction factor for a test section with plate and no solids present
f_{wall}	Friction factor due to the surface roughness of a pipe wall
F	Driving or resisting force
F_N	Wall normal force
F_N②	Two-solid model wall normal force
Fr	Froude number, $V/\sqrt{gD}$
g	Gravitational acceleration
H	Height of channel
j	Hydraulic gradient
j_m	Hydraulic gradient for a mixture
j_o	Hydraulic gradient for carrier fluid
j_{os}	Hydraulic gradient for carrier fluid at solids slip-point
j_p	Hydraulic gradient for plug flow
j_R	Hydraulic gradient for fines-affected carrier
j_s	Hydraulic gradient for solids slip-point

Symbol	Description
k	Constant in Equation (3.9)
L	Pipe Length
M^*	Mass flow ratio, $M^* = M_s/M_f$
M_f	Fluid mass flow rate
M_s	Solids mass flow rate
n	Constant in Equation (3.9)
ΔP	Pressure drop
ΔP_{bed}	Pressure drop in an all-steel test section with solids bed present
ΔP_{plate}	Pressure drop in a test section with a plate and no solids present
P_s	Static pressure
$\dot{Q}$	Fluid volume flow rate
q_{s1}, q_{s2}	Relative solids fraction
Re	Reynolds number, $Re = \rho VD/\mu$
S	Specific gravity
v_{s1}, v_{s2}	Solids volume
v_s	Total solids volume
v_T	Total volume
V	Equivalent throughput velocity
V_a	<u>In situ</u> fluid velocity in region above bed
V_b	<u>In situ</u> solids velocity in bed region
V_{mp}	Velocity at minimum hydraulic gradient
V_R	Relative velocity, $V_R = V_b/V_a$

Symbol	Description
V_s	Solids velocity
V_t	Turbulent suspension velocity
W	Width of channel
W_N	Submerged weight
W_N②	Two-solid model submerged weight
w	Free fall velocity
$\bar{w}$	Size fraction weighted average free fall velocity
x	Solids fraction between sequential sieve sizes
X	Dimensionless hydraulic gradient, $X = j_o/j_p$
X_s	Dimensionless slip-point hydraulic gradient, $X_s = j_{os}/j_p$
X_{sm}	Dimensionless hydraulic gradient at the maximum slip-point loci, $X_{sm} = (X_s)_{max}$
Y	Dimensionless hydraulic gradient, $Y = j/j_p$
Y_s	Dimensionless hydraulic gradient at slip-point, $Y_s = j_s/j_p$
α_R	Turbulent suppression factor
β	Solids bed angle
μ	Carrier fluid viscosity
μ_R	Relative viscosity of fines-affected carrier fluid
μ_s	Coefficient of sliding friction
χ	Particle shape factor
ξ	Friction factor ratio, $\xi = f_i/f_o$
ρ	Fluid density
ρ_m	Mixture density

Symbol	Description
ρ_R	Relative density of solids-affected carrier fluid
ρ_s	Solids density
τ_i	Interface shear stress at solid-liquid interface
τ_o	Shear stress of carrier fluid on pipe wall
②	Superscript denotes two-solid model parameter

FY-1979 PROGRESS REPORT
HYDROTRANSPORT PLUGGING STUDY

1.0 INTRODUCTION

The study described in this report is being conducted for the U.S. Department of Energy under direction of the Division of Fossil Fuel Extraction. The study in an outgrowth of a recognized need for a means to predict nominal operating conditions conducive to plugging for transport of large particle solids in a pipeline. A primary application of interest is the pipeline transport of coal from the mine face to a surface preparation plant.

Hydrotransport of coal in a mine offers health and safety advantages. Coal dust levels are decreased, thus reducing the potential for explosions. Reduced dust levels also provide a healthier work environment for miners. However, to compete with more conventional haulage systems such as conveyors or rail cars, hydrotransport must be economical.

Operation of a hydrotransport system can be economical if pumping costs are minimized while delivered solids are maximized. These conditions correspond to optimization at a low throughput velocity and high solids concentration. Unfortunately, these conditions correspond to a situation that may lead to pipeline plugging. Since a plugged line results in lost productivity, it is desirable to minimize such occurrences.

An adequate operating margin of safety can be designed into a hydrotransport system when adequate predictions of plugging can be obtained. The objective of this project is to provide an improved understanding of the parameters and phenomena that affect plugging predictions. This will result in improved modeling techniques and, subsequently, improved basis for design.

The Hydrotransport Plugging Study is being conducted by the Pacific Northwest Laboratory in four tasks, including:

- Review and Analysis of Current Prediction Capabilities and Available Data - The primary goal of this task was to review previous work performed to model the effects of flow regime, solids size characteristics, fines, turbulent suspension, and geometry on plugging and its prediction. This review was performed to provide the background and basis for work to be conducted in subsequent tasks.
- Analytical Modeling - The primary goal of this task is to develop improved prediction capabilities for large particle, run-of-mine coal transport.
- Experimental Investigations - The primary goal of this task is to perform small-scale experiments designed to isolate particular flow phenomena and obtain data supportive of analytical modeling efforts.
- Unplugging and Static Start-up - The purpose of this task is to identify and evaluate methods of unplugging a large particle pipeline and methods to enhance static start-up.

This report presents results accomplished to date in each of the four task areas. Conclusions permitted by these results are included and recommendations for future work are suggested.

2.0 CONCLUSIONS AND RECOMMENDATIONS

The primary goal of the first task was to review pertinent parameters, current predictive capabilities, and available data. Information gathered in this review led to the following conclusions and recommendations.

- Recent developments in the area of mechanistic modeling, which describe flow conditions at the limit of stationary deposition, provide the best basis for prediction and extrapolation of large particle flow. Based on a force balance analysis on a bed load in a pipe invert, the model can be used to predict the point of stationary deposition and operational characteristics for sliding bed flow with suspension in the carrier fluid above the bed.
- It was concluded that certain mechanistically modeled phenomena require further analytical evaluation to improve confidence levels for plugging predictions in large particle hydrotransport. Mechanisms of turbulent suspension, interfacial shear, and throughbed fluid flow are candidates recommended for improvement. Sensitivity of model predictions to these phenomena needs to be evaluated.
- Experimental work must be performed to support modeling and provide data for comparison. Small-scale testing designed to isolate phenomena and able to complement the applicability of the model should be performed. Two specific small-scale test related to this project's concern for large particle coal transport are recommended. These are determination of the coefficient of sliding friction of coal and rock in an underwater state and acquisition of data to support the modeling of interfacial shear.
- No available model is capable of treating a mixture of solids such as coal and rock, other than assuming a uniform mixture with corresponding mixture properties. This approach has not been demonstrated to be adequate, particularly in regard to the possibility that stratification of the light and heavy solids may lead to a quite

different incipient point of plugging. A recommended approach is to treat this stratified two-solid problem in a manner similar to the single-solid force balance approach.

Analytical modeling efforts based on the above conclusions and recommendations are in progress or planned for FY-1980. Initial work on developing a stratified two-solid limit of stationary deposition model has been completed. Conclusions and recommendations include:

- The stratified two-solid limit of deposition model contains the advantages of the single-solid mechanistic model. It is recommended that this model be further developed and extended to include prediction of operational characteristics of hydrotransport systems. Assumptions made in the derivation need to be further evaluated.
- There are no experimental data for stratified two-solid flow to which model predictions can be compared. Consequently, it is recommended that small-scale two-solid experimental tests isolating particular phenomena be designed and conducted to complement the modeling approach.

The experiment to measure the coefficient of friction of submerged coal and rock was completed. The conclusions reached include:

- The coefficient of friction was 0.5 ± 0.05 for submerged coal in both rusty and clean commercial steel pipe. No particle size dependence was found for the narrow size ranges tested for $0.05 < \bar{d}/D < 0.20$.
- The coefficient of friction for coal was particle size-dependent in smooth PVC pipe. Results were typically 40% less than in the steel pipe and were fit to $\mu_s = -0.69\ (\bar{d}/D) + 0.39$ over the range $0.05 < \bar{d}/D < 0.20$.
- Coefficient of friction results for crushed rock did not show any particle size dependence in either steel or PVC pipe and were typically 10% higher than the coal results.

- Results for dry sliding were higher than for submerged sliding, thus indicating a lubrication effect.

The coefficient of friction results are recommended for use in the mechanistic slip-point model to predict plugging. The recommended experiment to investigate interfacial shear and modeling approach is planned for FY-1980. The combined results of these two experiments will provide a basis for improved prediction of hydrotransport plugging.

3.0 REVIEW AND ANALYSIS OF CURRENT PREDICTION CAPABILITIES AND AVAILABLE DATA

Economical operation of a hydrotransport system designed to transport run-of-mine coal from the face to the surface or preparation plant is dependent on many factors. One important economic factor is that maximum solids throughput must be obtained with minimum energy consumption. This condition inherently requires, among other things, the combination of a large volumetric concentration of solids with low throughput fluid velocity. This combination is conducive to causing holdup in a pipe, resulting in a lower delivered rate of solids, and can lead to plugging, a situation in which no solids are delivered. A system design should avoid this situation since it would result in lost productivity. For a hydrotransport system to be designed properly to avoid plugging and reduce holdup, it is necessary to be able to predict when these conditions occur.

This section is concerned with the first of the project tasks. The objectives of the first task include:

- identification and analysis of the significant parameters causing or leading to the occurrence of holdup and plugging
- a review of current predictive capabilities and their applicability to run-of-mine coal transport
- a review and analysis of available data with specific concern for large particle-to-pipe diameter ratios
- identification of areas in which further experimental and analytical work needs to be performed.

In subsequent sections of this report, pertinent aspects of the phenomena associated with predicting hydrotransport characteristics are discussed. Although the first task is oriented most specifically toward analyzing the factors leading to plugging, the factors are necessarily analyzed in relation to the flow characteristics in general. Then, where appropriate, specific references to plugging factors are incorporated.

3.1 FLOW CHARACTERISTICS AND DEPENDENT PARAMETERS

Hydrotransport analysis is complicated by the large number of variables upon which the flow characteristics may depend. Since the objective of a designer is to predict pressure gradients and ensure plugging will not occur in a system, the variable dependencies of the flow characteristics must be known. In the case of single-phase flow, the gradient is a function of five variables: the pipe diameter and roughness, velocity, density, and viscosity. These variables can be combined to yield two dimensionless numbers, the Reynolds number and the relative roughness. In addition, only two flow regimes--laminar and turbulent--exist.

By comparison, in solid-liquid flow, the number of variables that may be needed to predict pressure gradients can easily be extended to fifteen. These include pipe diameter, roughness and slope, fluid density, viscosity and velocity, solids density, velocity and size, size distribution, shape, shape distribution, coefficient of restitution, concentration, and the gravitational constant. Numerous flow regimes also must be delineated. Thus, hydrotransport analysis can rapidly become an untenable task; simplifying assumptions must be made to adequately model hydrotransport and predict pressure gradient or plugging.

This section reviews background material important to understanding the principal phenomena associated with predicting plugging. This material includes flow regimes, characterization of solids size and motion, turbulent suspension, effects of fines, and effects of geometry. A review of these subjects provides the basis for analysis of prediction models made in Section 3.2. In that section, it is shown how flow regimes are mechanistically modeled to predict plugging.

3.1.1 Flow Regimes

In early work on slurry transport of solids, it was determined that certain distinct flow regimes could be discerned and that description of these regimes and their boundaries would suffice in describing the flow characteristics (Newitt et al. 1955, Turian and Yuan 1977). The regimes are commonly

depicted as shown in Figure 3.1. In actuality, demarcation between the regimes is not very clear and most certainly depends upon a number of flow parameters. Actual determination of the point of transition from one type of flow to another is also somewhat arbitrary since it is generally obtained from visualization experiments. Visual observations of two researchers may not exactly coincide when observing the same flow. This has been noted to be especially true in murky flows.

Most recently, Lazarus and Nielson (1978) attempted to compile a more descriptive chart of the possible flow regimes for horizontal pipe flow. They presented their results in a schematic form as shown in Figure 3.2. As can be seen from the figure, there is a complexity of possible regimes. The exact demarcation between regimes is not clearly defined although it is fairly easy to conceptualize the dividing line between where a bed exists and where no bed exists. Furthermore, the no-bed flow can be broken down into two-phase flow or single-phase flow regimes, depending upon the nature of the solids and the nature of the carrier fluid. Single-phase flow would behave differently, depending upon whether it can be characterized as a settling or nonsettling flow, in which case it may be non-Newtonian.

The bed-flow regime is of primary interest in this work. As the flow velocity decreases, larger suspended solids tend to transcend through a saltation mode, settle, and begin sliding along the pipe invert. At some velocity, the sliding friction force will become large, relative to bed driving forces, and a plugged pipe is imminent.

The mechanism by which the bed is initially formed may be crucial to predicting plugging. Kao (1976) has presented experimental evidence indicating that transient reinitiation of slurry flow from a stationary bed will not necessarily resume the same regime characteristics as were observed for steady-state flow subjected to the same pressure gradient. This may suggest that the mechanisms associated with formation of a stationary bed by decreasing velocity may not necessarily be similar to reinitiation by increasing velocity. The time rate of change of velocity may also have an effect and one might even argue that there is a hysteresis effect. Unfortunately, little to no

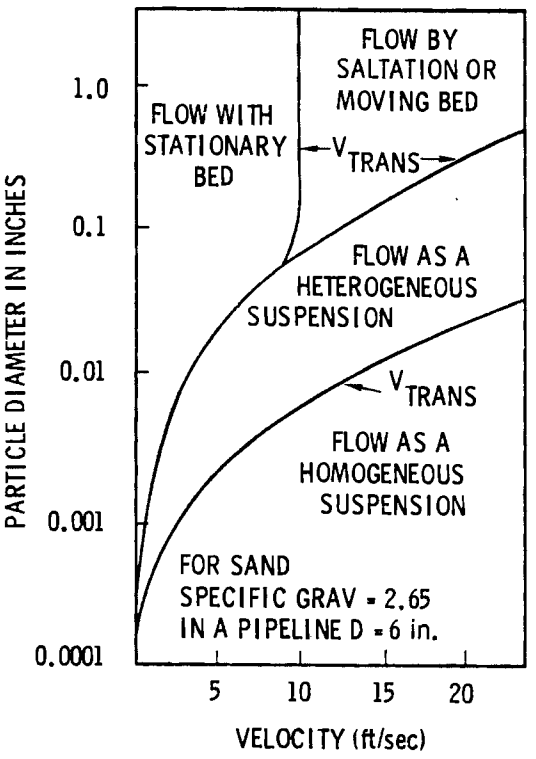

FIGURE 3.1. Slurry Flow Regimes (Newitt et al. 1955)

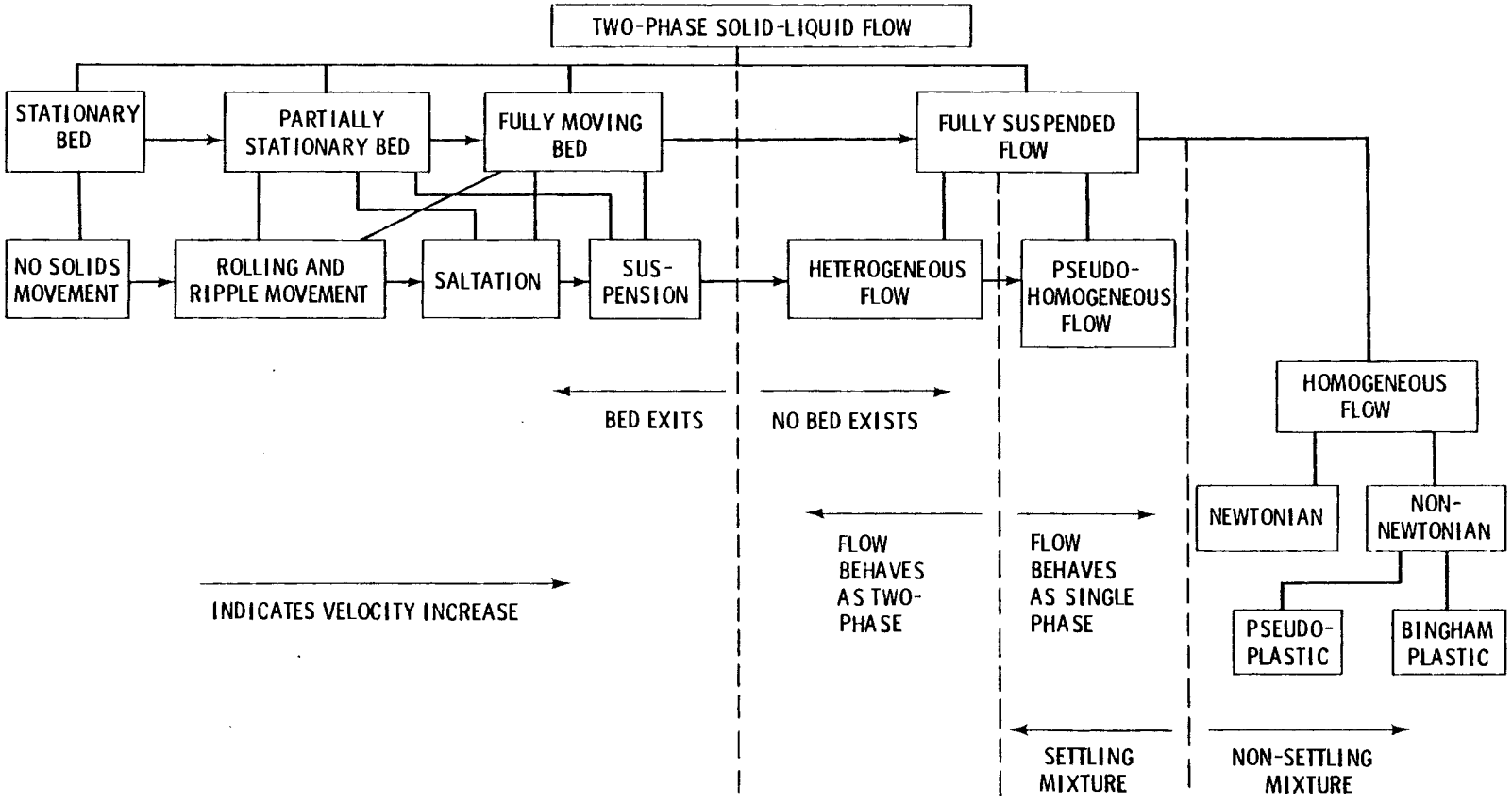

FIGURE 3.2. Flow Regimes for Horizontal Solid-Liquid Flow (Lazarus and Nielson 1978)

experimental data other than Kao's are available to support these contentions. While it might be useful to investigate these ideas further at a later time, the idea of transient experiments might well be postponed until a better understanding of basic steady or quasi-steady hydrotransport is obtained.

3.1.2 Characterization of Solid Particle Size and Motion

To characterize the motion of particles in a hydrotransport system, a number of aspects must be considered. These include description of single particle motions through fall velocity and drag coefficient, description of a distribution of particles through a characteristic size or sizes, and description of mechanisms leading to suspension of particles in turbulent flow. These aspects are discussed in this section.

The net motion of a single particle will be the result of the forces acting on the particle. Certainly the simplest motion to analyze is the free fall of a spherical particle in a quiescent fluid. In this case, the motion of the particle can be described by its free fall velocity as

$$w = \left[\frac{4}{3}\frac{gd(S-1)}{C_D}\right]^{1/2} \tag{3.1}$$

where the drag coefficient, C_D, is dependent on size and velocity. Even for a single spherical particle, free fall velocity must be determined iteratively. For nonspherical particles, the shape and surface characteristics become important in determining the drag coefficient. Alger and Simons (1978) have reported a shape factor correction for drag coefficient but their proposed correction would be extremely difficult to apply to particles with gross surface irregularities. Free fall of multiple particles is further affected by particle-particle interactions. Kazanskij (1976) and Wong and Liu (1972) have analyzed these interactions in some detail. They concluded that the free fall velocity in multiple particle systems may be decreased up to 30%; however, their analysis cannot yet be readily incorporated into an easily usable model for hydrotransport.

Determination of the fall velocity is important in modeling hydrotransport since it is used in numerous models that describe a criterion for minimum transport velocity. Alternatively, turbulent suspension flow is also tied to fall velocities. However, as a result of the innumerable difficulties inherent in describing actual motion of individual particles, gross simplifications must be made when attempting to model cumulative effects. For particles with uniform size, this can be done with some certainty. However, for solids with a large size distribution, for most model predictions it is necessary to assume that a characteristic dimension can be used to describe the distribution and, correspondingly, the cumulative effects of the solids distribution.

The most common method of determining a characteristic dimension is to perform a screen analysis of the solids. From this analysis, the characteristic dimension used to describe the solids could be defined as the screen size that allows 50% of the particles to pass through. Another would be the screen size corresponding to the largest fraction of solids passed. However, these are not always satisfactory and some sort of average size may provide a better alternative. The problem with screen sampling is that it is a measure of size in only two dimensions. Elongated pencil-like solids may lead to blockages, a problem encountered by Link et al. (1977) in their oil shale transport study.

Weidenroth (1978) has reported good success using a sieve fraction weighted average,

$$\bar{d} = \frac{\sum_{i=1}^{N} x_i d_i}{\sum_{i=1}^{N} x_i} \quad , \tag{3.2}$$

where x_i is the fraction of solids passing through sequential sieve openings. A correspondingly defined average fall velocity can then be determined as

$$\bar{w} = \frac{\sum_{i=1}^{N} x_i w_i}{\sum_{i=1}^{N} x_i}. \qquad (3.3)$$

These fraction weighted averages attempt to take into account the effect of size distribution. However, their use still inherently assumes that a single size can be used to characterize the overall distribution of solids. For widely varying distributions containing a significant percentage of large as well as small particles, a single averaged size may not be sufficient.

As an alternative, in a mechanistic model developed by Wilson (1976) it is suggested that a particular solids size distribution may be broken into fractional increments with each fraction characterized by an average size. This approach, which has been used in conjunction with his sliding-bed model discussed in Section 3.2.2, offers a potential advantage over a single averaged size. The advantage is that suspension of smaller particles may be treated separately from sliding or saltation effects of larger particles.

3.1.3 Turbulent Suspension

The need to understand particle suspension is based on observation that excess head losses in hydrotransport are dependent on flow regime. Determining flow regimes and, hence, points of transitions between regimes, is thus important. Newitt et al. (1955) developed an expression for the velocity where transition occurred between flow without suspension and heterogeneous suspended flow. Their expression was simply a function of the particle's fall velocity, or

$$V_t = 17\ w, \qquad (3.4)$$

where the fall velocity, w, is determined using either Equation (3.1) or (3.3). Other investigators recognized that the indirect influence of the particle

diameter on the free fall velocity, w, was not sufficient to describe its influence and that a more fundamental analysis of support mechanisms was needed.

Turian and Yuan (1977) performed an extensive analysis of flow regimes and prepared a regression analysis equation marking the transition velocity between sliding bed and heterogeneous flow. Their equation is given by

$$V_t = \left[2.411 C_d^{0.2263} f_o^{-0.2334} C_D^{-0.3840} Dg(S-1)\right]^{1/2}. \tag{3.5}$$

They also developed similar regression curves for transition between other regimes such as those shown in Figure 3.1.

Other work has shown that the ratio of the energy containing turbulent scales, ℓ, to the particle size, d, is very important in determining turbulent supporting mechanisms. Along this line, Wilson (1972) embarked on an analysis to determine the influence of the particle diameter on the velocity where suspension occurs, or the so-called transition velocity. He proposed

$$V_t = \frac{200\ wd}{\sqrt{f}\ D}, \tag{3.6}$$

where f is a clear water pipe friction factor and D is the pipe diameter. Later, Wilson and Watt (1974) attempted to improve the earlier model and proposed

$$V_t = 0.6\ w \sqrt{\frac{8}{f}} \quad \left[e^{(45\ d/D)}\right]. \tag{3.7}$$

This expression was reportedly based on several different sets of independent experimental results but subject to a relatively small ratio of $d/D \lesssim 0.03$.

By way of example, consider the oil shale work of Link et al. (1977). For their "C" shale and typical reported values of $\bar{d}/D \approx 0.07$, $w \approx 0.6$ m/sec, $f = 0.02$, Equation (3.7) predicts $V_t \approx 170$ m/sec, which seems abnormally

high. Typical experimentally observed saltation values were in the range of 3 m/sec. It is difficult to comprehend that suspension would require a fifty-fold increase in velocity. By comparison, Newitt's expression results in V_t = 10 m/sec, which is only a threefold increase over the observed saltation velocity.

Newitt's model for V_t, which effectively neglected direct effect of particle diameter, was based on experimental observations in numerous sand/water flows with a small d/D. Wilson's models attempted to account for turbulence energy length scale. However, in doing so, he essentially neglected any effect that the presence of the particles might have on the turbulent field and the energy length scale. The constants in his model (0.6 and 45) were obtained from data comparisons, which, as previously noted, were for $d/D \lesssim 0.03$. After Equation (3.7) was developed, its shortcomings were recognized. Current work is being conducted to improve the transition velocity estimation (Judge 1979). The importance of knowing V_t will become more apparent in a subsequent section, where it is used in relation to predicting hydrotransport characteristics of plugging in a combined bed and suspension flow.

3.1.4 Effect of Fines

Pumping large particles in a hydrotransport system may or may not be affected by the presence of fines. Determining the effect of fines on pressure drop and deposit velocity has been the subject of numerous investigations involving aspects of turbulent suppression, homogenization, effective viscosity or rheological properties, and wall friction. Most of the work has been related to sand-water flows although coal has received some attention.

Scott and Young (1972) present a summary of guidelines for the general flow characteristics caused by the presence of fines. For sand flows, fines may generally be classed as particles less than 50 μm in diameter. Smaller particles will generally tend to cause property variations of the mixture. Shook et al. (1976) reviewed previous work on the determination of slurry properties containing coarse coal (clay-free) particles. They also presented

results that showed the effect of adding fine, inert particles. Hisamitsu, Shoji, and Kosugi (1978) determined the effect of adding clay and limestone powder to sand-water settling flows. They found that the clay addition caused a reduction in minimum velocity and pressure loss but that the addition of limestone powder yielded only a slight reduction. Although their settling slurries were composed of relatively small particles (d_{50} = 150 to 800 μm), their flow reportedly remained Newtonian, even with the addition of the fines.

Sakamoto et al. (1978) presented results of limestone transport with coarse particles greater than 2 mm and fines less than 50 μm. They found that, for fines concentrations near 50 to 60%, particles in the range of 16 mm would not settle. Pressure losses and minimum velocity were reduced most when the fines concentration was near 30%. They concluded that a hydrotransport system using a return line to maintain high fines concentration could be a very effective means of transporting large chunks of coal. However, this is in an operational mode and system startup may cause additional problems if the rheology were such that a large yield stress of the fines mixture had to initially be overcome.

Another experimental effort worth noting, although very few experimental results are presented, is the work of Funk et al. (1978). While their main objective was to test a coal injector, they obtained some data on large particle (d_{max} = 100 mm) raw coal transport in a large pipe (D = 254 mm). The raw coal contained as much as 15% solids other than coal, most of which was rock. The experimental arrangement was such that the carrier fluid (so-called black water) was recirculated after the transported solids were removed. As a result, significant fines were continually present in concentrations up to 15 to 20% with some recirculated particles as large as 6 mm. Their work was injector-testing oriented. Consequently, flow data were considered secondary and no attempts were made to separately investigate or control the effects of fines. It is worthwhile to note that no plugging occurred in their transport line and restart was easily accomplished after a 2-month shutdown. The fines

present in their pipeline were due to natural causes such as diminution because the system was constructed so the large particles being transported did not pass through a pump.

Some interesting data on the production of fines are also presented by Haas, Husband, and Shook (1978). They measured the hydraulic characteristics of three different -19 mm coals in a 100-mm pipe. For a lignite coal, attrition and resulting fines production was primarily due to rounding of large particles. These fines typically had a median size of 5 μ with resulting fines concentrations ranging from 9 to 16%. Their Sheerness coal also produced fines by rounding attrition, but resulting fines concentration was only 2 to 7% after short-duration tests. However, after one continuous 4-hr run, fines in the Sheerness coal increased to 20%. The increase in fines caused a substantial increase in pressure drop from the beginning to the end of the test. The third coal tested was a McIntyre metallurgical coal. This material showed a much higher attrition than either of the other two, and indicated that particulate fracture was more dominant than rounding, which resulted in a more uniform diminution of the coal sample.

Although it may be extremely difficult, a priori, to know what amount of fines will be present in a system, there are proposed methods of considering their presence. Vocaldo (1976) suggests that accounting for the effective viscosity and density of a carrier-affected fluid is sufficient. He proposed that the hydraulic gradient in fines-affected flow would be a function of the relative viscosity, μ_R, the relative density, ρ_R, and the clear fluid gradient, j_o, or

$$j_R = j_o \alpha_R \left(\mu_R\right)^{2-t} \left(\rho_R\right)^{t-1} \quad . \tag{3.8}$$

The relative viscosity is given by

$$\mu_R = \frac{\exp\left[\left(kC_b - n\right) C_{Rh}\right]}{\left(1 - C_{Rh}\right)^n}, \tag{3.9}$$

and the relative density is the ratio of fines-affected mixture density to that of clear fluid, or

$$\rho_R = \frac{\rho_m}{\rho} . \tag{3.10}$$

The factor α_R is a turbulence suppression constant equal to 0.9 while t is the slope of a friction factor curve. C_b and C_{Rh} are the packed bed fraction (concentration) and the relative concentration of fines in suspension, respectively, while k and n are constants for a given solid/liquid combination. Using values of k = 4.0, C_b = 0.45 and n = 2.0, Equation (3.9) yields very good agreement with the modified Eiler expression proposed by Ferrini et al. (1978) and with Faddick's effective viscosity ratio data (1974) for coal-water mixtures.

3.1.5 Effects of Geometry

Determining the effects geometry has on hydrotransport is one area that has received relatively little attention. Analysis of flow parameters has been concerned primarily with horizontal flow, with lesser attention to vertical flow. This is reasonable in that vertical flow is a problem in which multiparticle drag coefficients is a main concern, whereas analysis of horizontal flow must be concerned with numerous other aspects.

Except for a few isolated endeavors, experimentation and analyses have been concerned only with circular pipes, again with justifiable reason. Two notable exceptions are the works of Wang and Seman (1973) and Sauerman (1978). Wang and Seman experimentally determined the hydraulic characteristics of flow in six cross section shapes: a circular pipe, a square pipe, a triangular pipe with the flat side both up and down, and a rectangular pipe with the long side oriented both vertically and horizontally. Uniform glass beads with d = 1.4 mm, S = 2.93, and w = 19.3 cm/sec were used. The cross-sectional area was the same in all pipes. They measured the primary hydraulic variables, namely headloss, velocity, and concentration. Wang and Seman concluded that minimum power requirements at their highest delivered concentrations

(C_d = 15.5%) were obtained for the rectangular pipe horizontally oriented with the long side on the bottom. At lesser concentrations, no geometry effect was discerned.

Sauerman more recently reported similar conclusions utilizing a segmented pipe—one in which a flat surface was welded into the invert of a circular pipe. Sand ($\bar{d}$ = 3 mm) and anthracite coal ($\bar{d}$ = 9 mm) were tested. Experimental results indicated that their segmented pipe resulted in lower power requirements when the flat plate was located across the chord at a vertical distance of one-third the diameter from the bottom of the pipe. For equal solids throughput, the segmented pipe required 16% less power than when pumped through a circular pipe without the flat plate. Interestingly enough, the segmented pipe also offers an advantage of the plate acting as a sacrificial wear plate.

Another important aspect of geometry is the slope of a pipeline. While the main implications concerning the slope are related to startup and shutdown, it can also be important in determining operational characteristics. Gandhi and Aude (1978) analyzed the time dependency of an interface in a settling slurry based on slope angle of a 7.6-cm pipe. They also presented some results of an experimental test on a large (D = 0.5 m) iron concentrate pipeline. Unfortunately, confirmation of their hypothesized bed formation model could not be made, due to experimental shortcomings in the large-diameter line.

In another investigation of pipeline slope, Masliyah and Shook (1978) analytically evaluated the characteristics of an idealized flow situation, which has basic application to a shutdown slurry pipeline. They examined the case of a laminar zero net flow where two different immiscible fluids were flowing countercurrent in a sloped geometry. They assumed this flow to be representative of a steady-state condition, which has application to a situation in which the counterflowing bed of solids exhibits relatively slow, sliding motion. In this case, their analysis would correspond to a quasi-steady flow and could be used to characterize shear flow near solid-water interfaces after shutdown of a sloped line.

Numerous other geometrical considerations, which would have some effect on hydraulic characteristics and thus, plugging, can also be envisioned. These could possibly include area variations created by valves, injectors, pump intakes, pipe-joint mismatching, and sharp elbows. Experience, common sense, and engineering judgment are the only guidelines that can be used for design of these situations.

3.2 PREDICTION METHODS AND DATA COMPARISONS

In this section, an analysis of currently available prediction methods is presented. These include empirical and regression curve fit models as well as recently developed mechanistic approaches. One of the main conclusions reached in this study is that the mechanistic approach offers the best potential for accurate plugging prediction over a wide range of parameters and flows. It is discussed in detail in Section 3.2.2.

3.2.1 Empirical Models

Numerous empirical models, which attempt to predict the hydraulic performance and minimum velocity of hydrotransport systems, have been developed. A commonly cited fault of nearly all of these models is that they are essentially no more than empirical curve fits of data taken over a limited range of the independent variables. Incorporation of physical processes is usually limited and, as a result, the models regularly fail to predict flow characteristics outside the range of data for which the models were developed.

In recent years, considerably more effort has been devoted to understanding the physical processes involved in describing solids motion, flow regime specification, and boundaries between flow regimes. As a result, better models, which are more generally adaptable to scale-up, plugging, and headloss prediction, are appearing.

It is not necessary to present an exhaustive comparison of minimum velocity prediction methods. Such comparisons can be found elsewhere [see, for example, Lazarus and Nielson (1978) or Šašić and Marjanović (1978)]. It will suffice to present a review of the results of such a comparison conducted

by Wiedenroth and Kirchner (1972). They compared the results of critical velocity predictions of 16 models for pipe diameters from 50 to 600 mm, concentrations from 5 to 30%, and characteristic sand and gravel (S = 2.65) particle sizes from 0.2 to 6 mm. However, of the 16 models compared, this author found errors or could not replicate the tabulated results for seven of the models reported. In another four models, unobtainable graphs in original publications were needed and thus could not be checked. In one case, it was even noted that their tabulated values did not correspond to their graphed results.

The wide scatter in the predicted critical velocity is best demonstrated by replotting their tabulated results (which were replicable) from the remaining five models and several obviously correctable models. Figure 3.3 shows the predicted minimum velocity as a function of delivered concentration for $\bar{d}$ = 6 mm and D = 0.1 m. Figure 3.4 shows the minimum velocity as a function of pipe diameter for C_d = 0.30 and $\bar{d}$ = 6 mm. Figure 3.5 shows the critical velocity as a function of characteristic particle size for D = 0.1 m and C_d = 0.30. As a further example, Figure 3.6 shows similar predicted results of minimum velocity as a function of solids specific gravity for the models.

It should be noted that the different models were originally obtained based on experimental results with particular solids and were not necessarily consistent even in their definition of what is herein called minimum velocity. Thus, the range of applicability of parameters for each specific model may not cover the range shown in Figures 3.3 through 3.6. Nevertheless, these figures point out that large variance in predicted results exists, making the designer's job all that much more difficult. It should also be pointed out that several other commonly referenced models, including Worster and Denny (1959) and Vocaldo and Charles (1972) were omitted from the comparison. Their inclusion is not expected to be of any added value. Myriads of other references to minimum velocity data and empirical correlations could also be made; however, there has yet to be found an empirical correlation that has withstood the test of time or generality.

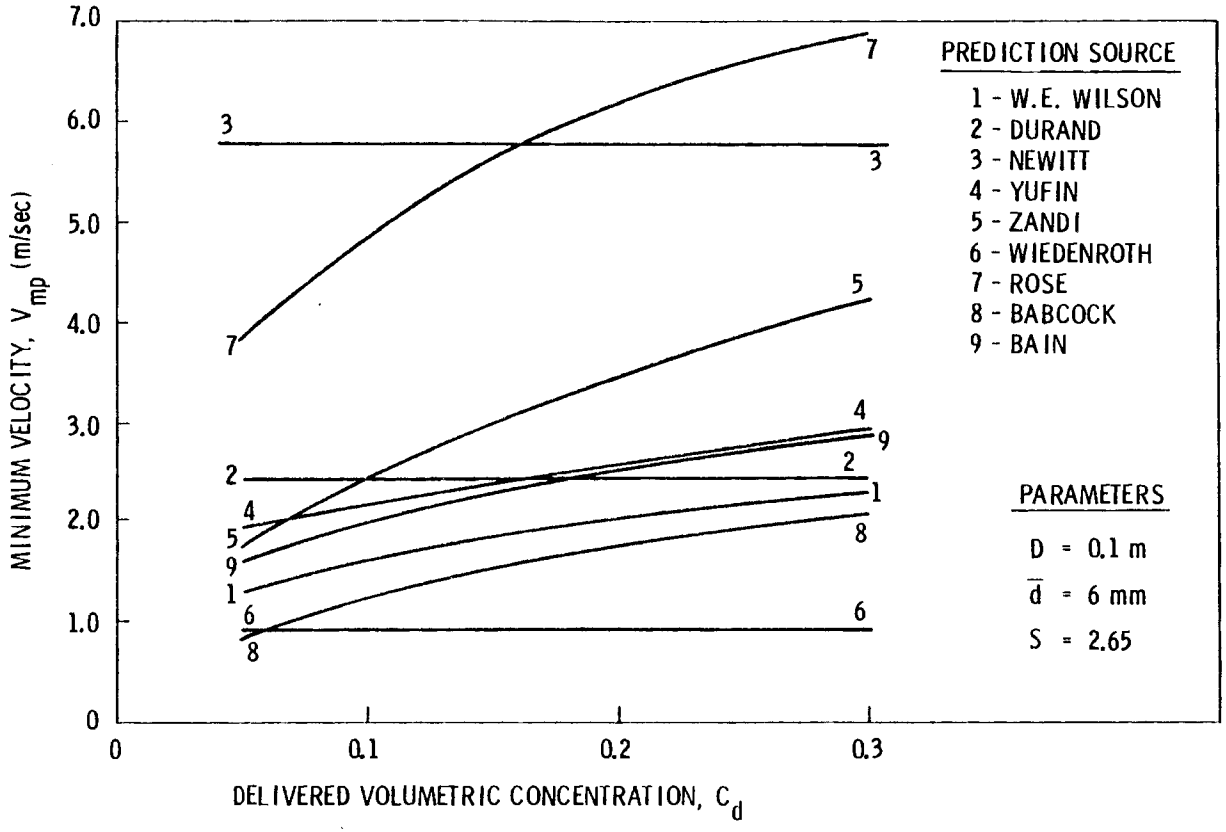

FIGURE 3.3. Comparison of Predicted Minimum Velocity Dependency on Concentration

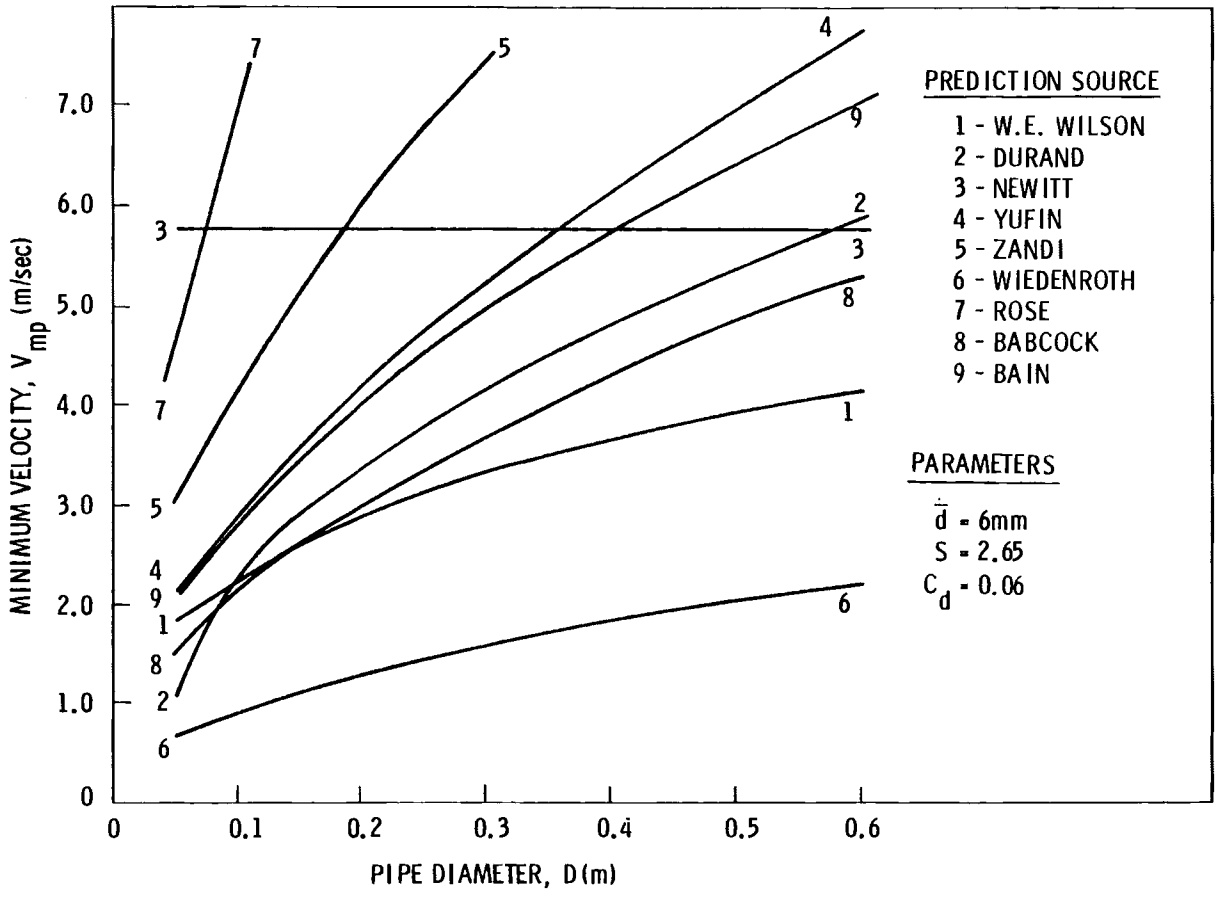

FIGURE 3.4. Comparison of Predicted Minimum Velocity Dependency on Pipe Diameter

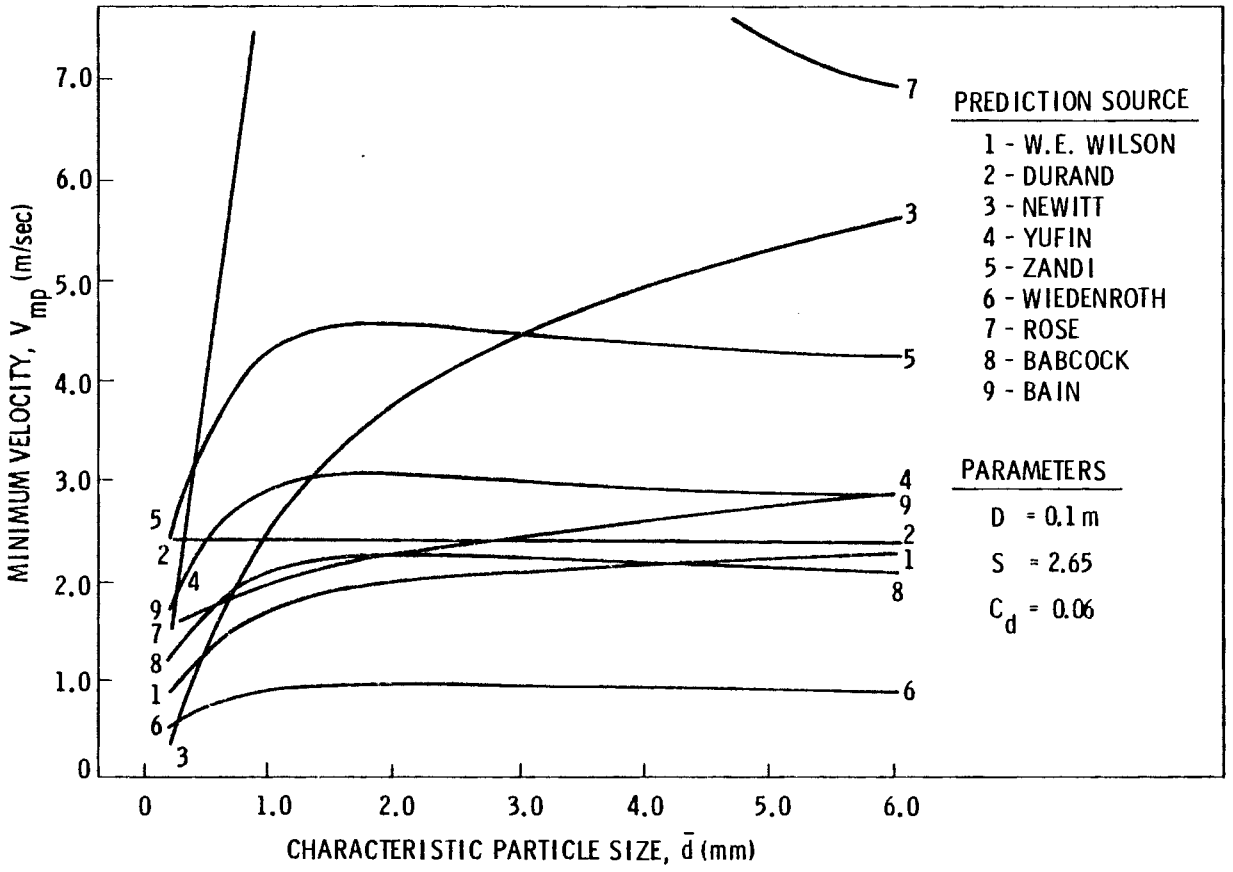

FIGURE 3.5. Comparison of Predicted Minimum Velocity Dependency on Characteristic Particle Size

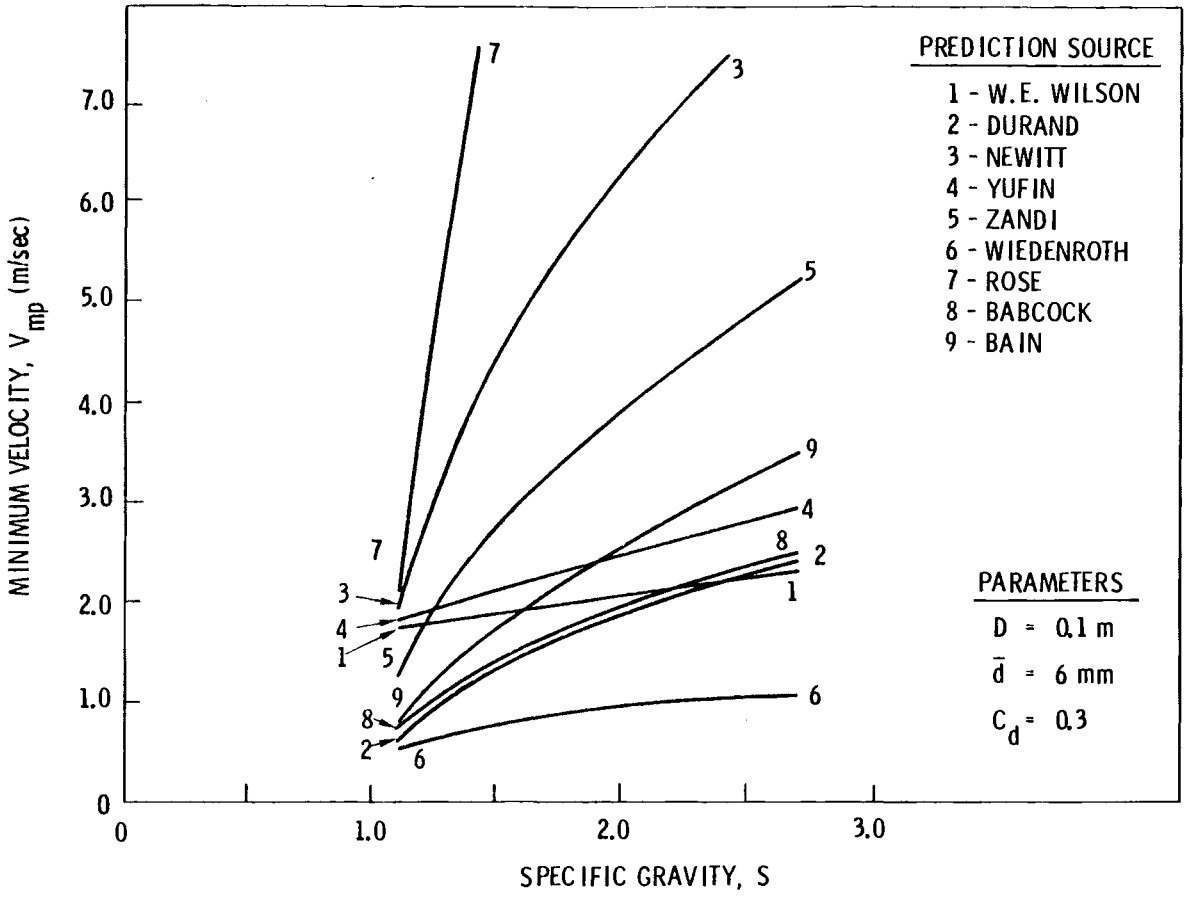

FIGURE 3.6. Comparison of Predicted Minimum Velocity Dependence on Specific Gravity

Perhaps one reason for the development of so many models at large variance with each other is disagreement of data trends. For example, consider the data of Carleton et al. (1978) and the oil shale data of Pouska and Link (1978). In the former study, limestone aggregate and colliery spoil were transported in narrow and wide size ranges up to -50 mm in a 157-mm pipe. Their results are shown in Figure 3.7. The latter study transported oil shale with wide size ranges of -25 mm, -13 mm, and -4.7 mm in a 157-mm pipe. Their results are shown in Figure 3.8.

It is obvious that three different trends are present in Figures 3.7 and 3.8. For the narrow size range limestone, the data indicate a definite increase in pressure drop with decrease in particle size, whereas the wide range data show a maximum pressure drop occurring for the -10 mm size range. The oil shale data show a marked increase in pressure drop with increase in size range at a given concentration and throughput velocity.

It is interesting to note that similarly conflicting size effect data can be found in relation to attrition. Carleton et al. (1978) noted nearly a factor of two decrease in pressure drop after a 2-hr run with colliery spoil at 3.3 m/sec and $C_d = 0.10$. Haas, Husband, and Shook (1978) noted nearly a factor of two increase in pressure drop at a similar velocity and $C_d = 0.45$ for their Sheerness coal data. However, coal degradation tests in a 157-mm pipe did not show any noticeable variation in hydraulic gradient over a 30-min period.[(a)]

The extent to which efforts have been taken to develop these empirical models can be demonstrated by Lazarus and Nielson's (1978) work. They acquired a plethora of data mostly from the Saskatchewan Research Council. After analyzing the pertinent variables and obtaining five dimensionless parameters, they proceeded through an exhaustive curve fitting process to derive an expression to predict hydraulic gradient. Subject to the range of parameters listed in Table 3.1 they derived the model described next.

(a) These results were provided by A. J. Miscoe, U.S. Department of Energy, Pittsburgh Mining Technology Center, Bruceton, Pennsylvania.

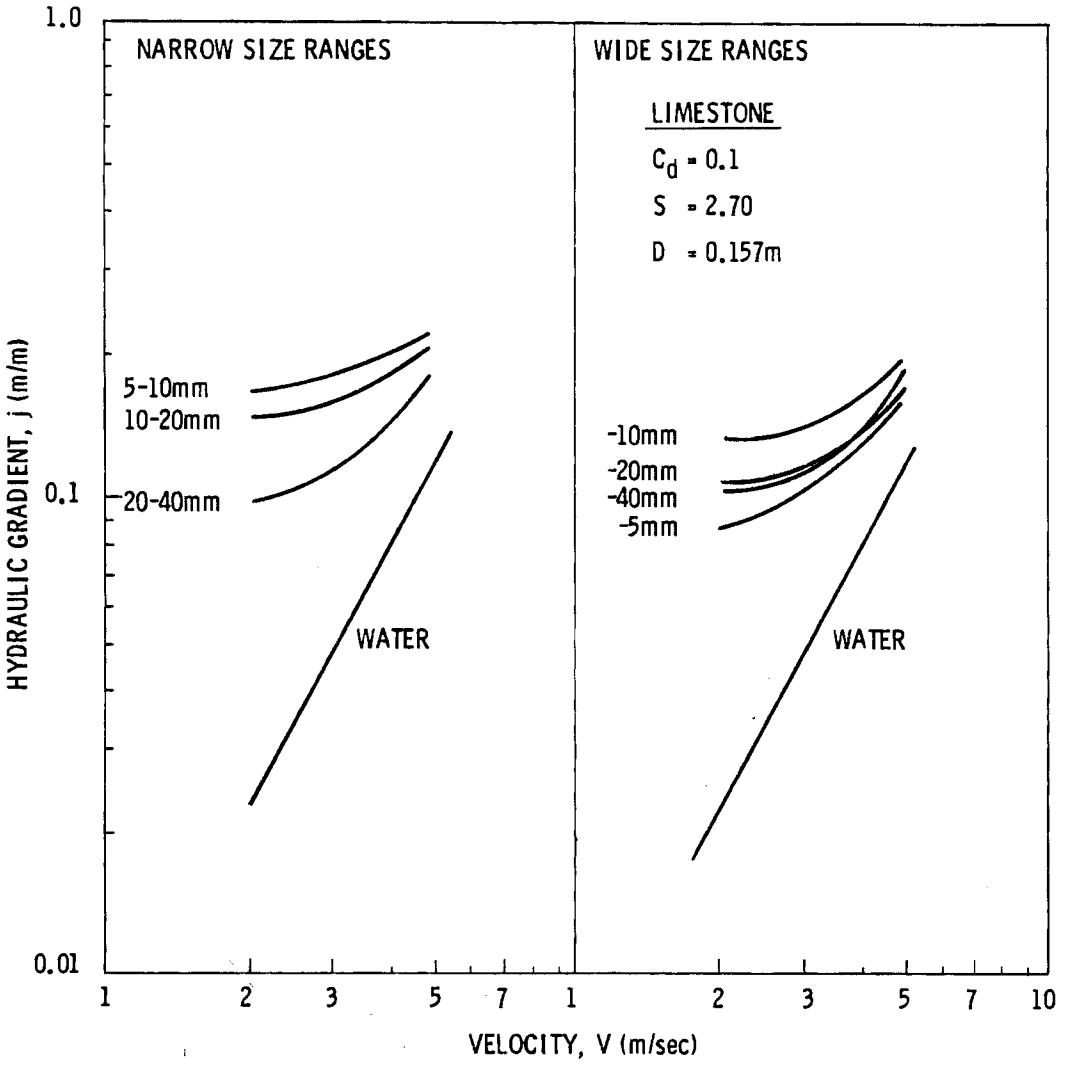

FIGURE 3.7. Narrow and Wide Size Range Transport of Limestone (Carleton et al. 1978)

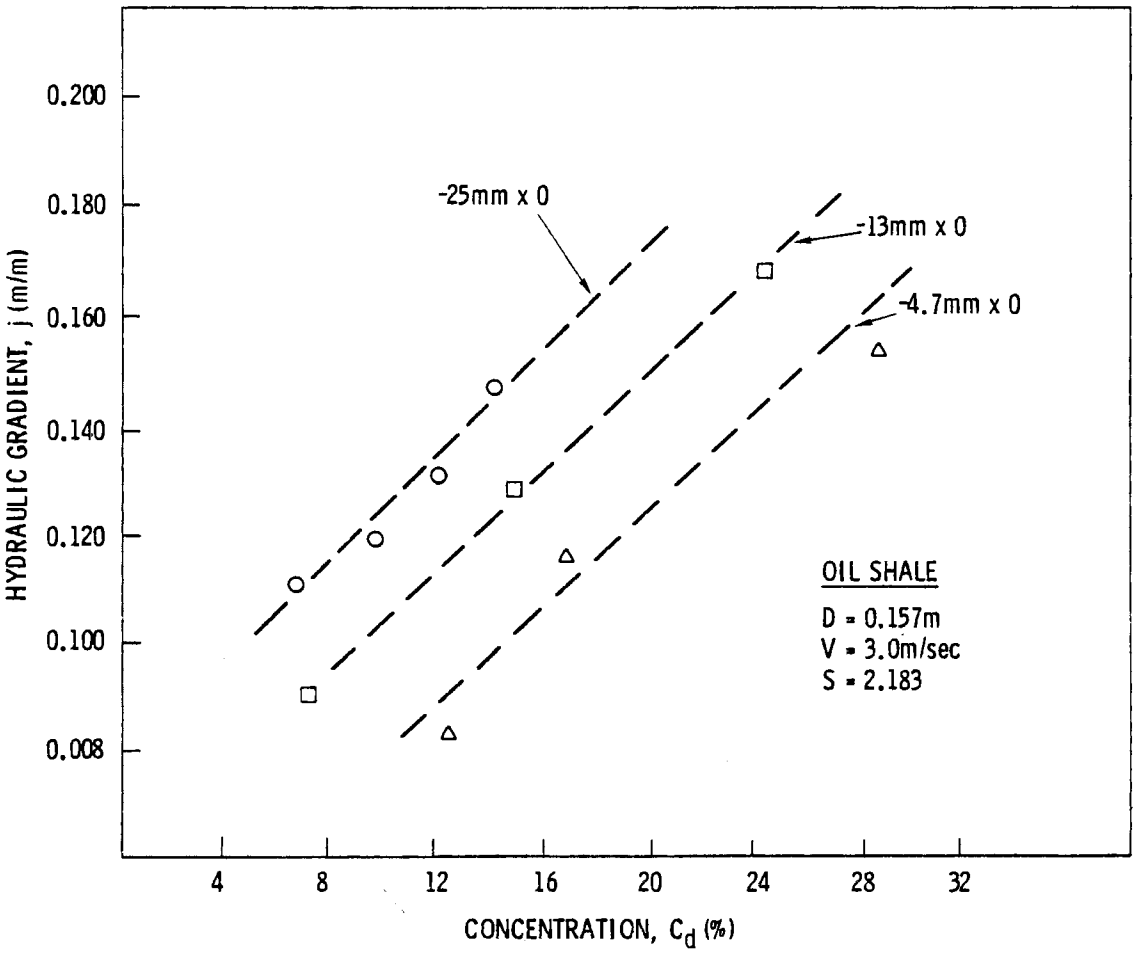

FIGURE 3.8. Wide Size Range Oil Shale Transport (Pouska and Link 1978)

TABLE 3.1. Scope of Investigation of the Lazarus and Nielson Correlation (Lazarus and Nielson 1978)

Variable	Symbol	Range	
		High	Low
Pipe diameter	D	315 mm	32 mm
Fluid density	ρ	1,132.6 kgm/m^3	982 kgm/m^3
Fluid viscosity	μ	0.0382 Pa-sec	0.000473 Pa-sec
Particle density	ρ_s	11,120 kgm/m^3	2,650 kgm/m^3
Average particle size	d	3.18 mm	0.032 mm
Reynolds number	Re	1×10^6	3×10^3
Mass flow ratio	M*	3.5	0.0
Relative density	S	11.12	2.34
Size ratio	d/D	0.1	0.0001

The friction headloss gradient, j_m, for uniformly sized particles in a smooth horizontal pipe was defined as

$$j_m = \frac{\Delta P}{\rho g L} = \frac{2 f_m V^2}{gD}, \tag{3.11}$$

where V is the nominal fluid velocity defined as fluid volume flow rate per unit area,

$$V = \frac{4\dot{Q}}{\pi D^2} \quad . \tag{3.12}$$

They then proceeded on the basis that the ratio of the mixture friction factor, f_m, and a base friction factor, f_b, is a function of the pertinent dimensionless numbers. The base friction factor is an asymptotic value approached at high velocity pseudo-homogeneous flow. The pertinent parameters

were the mass flow rate, $M^* = M_s/M_f$; the flow Reynolds number, $Re = \rho V D/\mu$; the size ratio, d/D; the specific gravity, S; and the Froude number, $Fr = V/\sqrt{gD}$.

The resulting curve-fit expression for the friction factor ratio was

$$\frac{f_m}{f_b} = 1 + 2.1\left(\exp\left[-2(\lambda-0.32)\right]\right) + 5.85\left(\exp\left[-12(\lambda-0.32)\right]\right), \tag{3.13}$$

where

$$\lambda = \frac{Fr^2}{S}\sqrt{\frac{1}{ReM^*}}\left[1{,}000\left(\frac{d}{D}\right)^{0.44\ \mathrm{Log}_{10}(\frac{d}{D})+1.31}\right]^{\tanh(1+M^*)}. \tag{3.14}$$

They also presented curve-fit results of

$$\mathrm{Log}_{10}(f_b) = -\alpha + \beta M^* - \gamma\exp\ (-2M^*) \tag{3.15}$$

where

$$\alpha = \exp\left[0.835 - (6.3 - \log_{10}Re)^2/24\right], \tag{3.16a}$$

$$\beta = \exp\left[(7-\log_{10}Re)^2/28 - 1.6\right], \tag{3.16b}$$

$$\gamma = (\log_{10}Re - 5.2)^2/24.5 + 0.2, \tag{3.16c}$$

and for clear water in a smooth pipe,

$$\log_{10}(f) = -(\alpha + \gamma).$$

Subject to the range of variables in Table 3.1, this model resulted in a log standard error of less than 4% of predicted versus measured pressure

gradients for over 1,100 data points. By comparison, other models (some of which are plotted in Figures 3.3 through 3.6) using the same data resulted in log standard errors of up to 76%, with largest scatter in low headloss gradients. Although Lazarus and Nielson did not attempt to predict minimum velocities, one could conceivably differentiate their expressions and determine the point at which dj_m/dV is zero, and hence, determine a criterion for a minimum velocity.

One problem with their model is that it is limited, at least in the derivation, to small uniformly sized particles with $S > 2.34$. It might be quite useful to determine if an extension to $S = 1.3$ (typical for coal) were possible and to determine if a characteristic size, say $\bar{d}/D$ or $d_{50}/D \leq 0.1$, could be used to predict gradients in which nonuniform size distribution of solids exists.

3.2.2 Sliding Bed Models

Having recognized several years ago that empirical curve-fit type models lacked general physical basis and an inability to be extrapolated or scaled up, several researchers have attempted to develop mechanistic models. Reportedly, the most successful of these are the so-called sliding bed models, which include the works of Wilson (1976), Televantos (1977), and Pouska and Link (1978). Since this type of modeling seems to offer significantly greater potential for scale-up calculations than the empirical models, it will be discussed in some detail.

Various publications related to the mechanistic sliding bed model developed by Wilson and co-workers can be traced back to 1965. Much older reference to experimentally observed sliding beds can also be found. Rudimentary basis and heuristic arguments concerning flow behavior and characteristics near the point of deposition can be found in a comparison made by Wilson and Brebner (1971) of pressurized (pipe) and unpressurized (open channel) flow. In reporting experimental data for sand-water flow, they presented evidence and a supporting heuristic argument contending that the deposition velocity did not necessarily monotonically increase with increasing concentration, thus countering most empirical models to date. In a series of publications,

Wilson, Streat, and Bantin (1972), Wilson (1972, 1974, 1976), Wilson and Watt (1974), and Wilson and Judge (1978) presented various stages of development of the slip-point/sliding bed models. Since the model is thought to be significant with respect to predicting plugging and hydraulic characteristics, it is discussed in some detail below. Subsequently, a similar approach proposed by Pouska and Link (1978) is discussed.

Consider a horizontal pipe in which solid particles exist at rest in the pipe invert with a fluid flowing in the upper portion of the pipe as shown in Figure 3.9. As the fluid velocity is increased, it can be envisioned that the bed will begin to slide when the driving force produced by the pressure gradient exceeds the mechanical friction between the bed particles and the pipe wall. Analyses of the forces on the bed and fluid are the bases for the slip-point/sliding bed models. It was previously pointed out that a number of flow regions exist between the limits of stationary bed and pseudo-homogeneous suspended flow (see Figure 3.2). However, it has also been noted that complete analytical description of all these regimes is currently impossible. The assumptions made in deriving the slip-point/sliding bed models represent a balance between complexity and realistically describable mechanisms.

The driving force on the bed is caused by the pressure gradient, j, and includes an interfacial shear force, $F_{\tau,i}$, and a force in the bed, F_j, equal to $\rho g j A_b$ per unit length. The resisting force, $F_{\tau,w}$, equals the coefficient of friction, μ_s, multiplied by the normal force exerted by the particles on the wall. The total driving force can be written as

$$F_{D,b} = F_j + F_{\tau,i}$$

$$= \rho g j A_p (1-a) + \tau_i D \sin \beta \qquad (3.18)$$

The resisting force can be written as

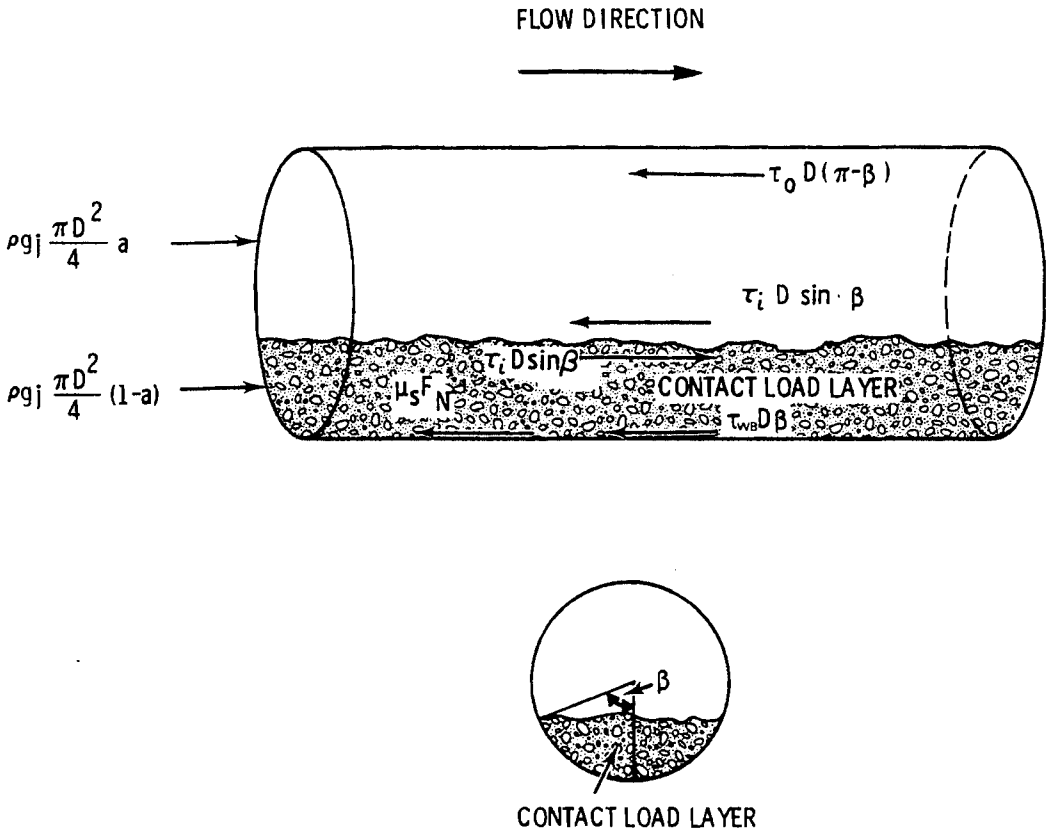

FIGURE 3.9. Geomtry and Forces Acting on a Stationary Bed-Load in a Pipe Invert

$$F_{R,b} = F_{\tau,w}$$

$$= \rho g j_p A_p \left(\frac{\sin \beta - \beta \cos \beta}{\pi} \right) \tag{3.19}$$

where j_p, the gradient required to move a packed bed filling the whole pipe, is used because it has been found (Wilson 1976) that

$$j_p = 2 \mu_s C_b (S-1). \tag{3.20}$$

The coefficient, 2, in this expression follows from the assumption that intergranular pressure causes an upward normal component in the pipe overt and C_b is the concentration of the packed bed while S is the specific gravity of the solids.

To solve the force balance of Equation (3.18), it is convenient to eliminate τ_i by defining a friction factor at the interface, or

$$\tau_i = f_i \rho \frac{V_a^2}{8}, \tag{3.21}$$

where V_a is the <u>in situ</u> velocity of the fluid above the bed.

Furthermore, it is necessary to perform a similar force balance on the fluid above the bed. The driving force is still caused by the pressure gradient, j, but two resistances exist. One is due to the fluid shear on the wall, τ_o, and the other is due to fluid shear on the interface, τ_i. Thus, for the fluid layer,

$$F_{D,o} = F_j = \rho g j A_p a, \tag{3.22}$$

and

$$F_{R,o} = \tau_o D(\pi - \beta) + \tau_i D \sin \beta. \tag{3.23}$$

At this point it is necessary to determine a relationship between τ_o and τ_i. By defining

$$\xi = \frac{f_i}{f_o}, \tag{3.24}$$

where f_o is the clear water friction factor, it can be shown that

$$\tau_i = \xi \tau_o \tag{3.25}$$

where

$$\tau_o = \frac{f_o \rho V_a^2}{8}. \tag{3.26}$$

The friction factor ratio, ξ, represents a means whereby the effect of solids particle size is incorporated. At this point it remains an unknown and will be discussed subsequently.

By eliminating τ_i in favor $\xi\tau_o$ in Equation (3.23) and equating $F_{D,o}$ to $F_{R,o}$ it can be found that

$$\tau_o D = \frac{\rho g j A_p a}{(\pi - \beta) + \xi \sin \beta}. \tag{3.27}$$

Using this expression in Equation (3.18), the driving force on the bed can be written as

$$F_{D,b} = \rho g j A_p \left[(1 - a) + \frac{a\,\xi \sin\beta}{\pi - \beta + \xi \sin\beta} \right] . \tag{3.28}$$

Furthermore, by equating the bed driving and resisting forces it can be shown that

$$\frac{j}{j_p} = \frac{\left(\frac{\sin\beta - \beta\cos\beta}{\pi} \right)}{(1 - a) + \frac{a\,\xi \sin\beta}{\pi - \beta + \xi \sin\beta}} . \tag{3.29}$$

The ratio, j/j_p, represents the ratio of the hydraulic gradient at the point where the bed begins to slip to the hydraulic gradient required to move a packed bed filling the whole pipe. This ratio can be defined as

$$Y_s = \frac{j_s}{j_p} = F(\beta,\xi) \tag{3.30}$$

where the subscript s is added merely to indicate the gradient of the point of slip. It can be noted that the gradient ratio, Y_s, is a function only of β and ξ and is only of limited practical use at this point since β is generally unknown.

To eliminate the explicit dependence of β, consider the fluid layer above the bed. The fluid velocity, V_a, can be related to an equivalent throughput velocity, V, as

$$V_a = \frac{V}{a} \tag{3.31}$$

where a is the area fraction occupied by the clear fluid above the solids bed. Using this definition, the last term in Equation (3.23) can be written

$$\tau_i D \sin \beta = \xi \tau_o D \sin \beta$$

$$= \rho g \frac{f_o V^2}{2gD} \frac{A_p \xi \sin \beta}{\pi a^2}$$

$$= \frac{\rho g j_o A_p \xi \sin \beta}{\pi a^2} \tag{3.32}$$

where j_o is the equivalent hydraulic gradient that would result if an equal discharge of fluid existed from the whole pipe and is denoted as j_{os} at the point of slip. Using Equation (3.32), the balance on the bed can be written as

$$Y_s(1 - a) + X_s \frac{\sin \beta}{\pi a^2} = \left(\frac{\sin \beta - \beta \cos \beta}{\pi}\right). \tag{3.33}$$

The ratio

$$X_s = \frac{j_{os}}{j_p} = F' \left(\beta, \xi, Y_s\right) \tag{3.34}$$

represents the ratio of the equivalent clear water throughput gradient to the gradient required to move a packed bed.

The ultimate result of this slip-bed model is a locus of points in the Y_s versus X_s plane. This locus represents the limit of the stationary deposit zone and is only a function of ξ, the friction factor ratio f_i/f_o, and β, the bed angle that can be directly related to in situ concentration, C_i.

It can be argued that the friction factor at the surface of the bed will be a function of the ratio of particle diameter to pipe diameter in a manner similar to determining effective roughness of a pipe. Thus, Wilson (1976)

proposed assuming ξ can be determined as twice the value determined from Nikaradse's formula for pipe friction factor with fixed grain roughness. Therefore, ξ may vary from 2 for a smooth pipe to 20 for d/D = 0.20. Furthermore, Wilson proposed that variations of the model with ξ could be effectively eliminated by plotting the excess gradient due to sliding bed resistance, $(Y_s - X_s)$, versus the ratio of equivalent clear water gradient to the equivalent clear water gradient at the maximum point of the slip locus, X_s/X_{sm}. The resulting generalized slip-point gradient correlation is shown in Figure 3.10. Subject to the assumptions of the model, the results shown in Figure 3.10 may be used to define lower limits of operation. Transfer to the more common $\Delta P/L$ versus V coordinates is accomplished directly through definitions of the axes, $(Y_s - X_s)$ and X_s/X_{sm}, respectively.

It may be useful to clarify a few aspects related to assumptions made in the model. The coordinates Y_s and X_s have physical meaning. Y_s is defined such that there are specific limits as to its value. In the upper limit, as the solids concentration increases up to a maximum of C_b, the limiting case of the plug flow exists, or $Y_s = 1$. The excess gradient due to the solids bed has to decrease to zero as concentration decreases or, equivalently, return to the case of clear water flow. In between, a maximum corresponding to X_{sm} must occur.

The X_s and Y_s coordinates are also readily convertible to the more commonly used coordinates, $\Delta P/L$ versus V. Specific flow properties are needed to permit this conversion. The friction coefficient, μ_s, and packed bed fraction, C_b, are perhaps the most nebuluous values required. They may be determined for particular situations through relatively simple experimentation. As an upper limit, one might let C_b be the maximum packing factor for uniform spheres. Consistent specifications may be more difficult (and subject to wide variation) if a wide range of particle sizes existed such that small particles could fill the gaps between larger particles. Similarly, while determination of μ_s may be accomplished with relatively simple experimentation, the range and effect on μ_s of such things as particle size, bed depth, and surface roughness may be necessary.

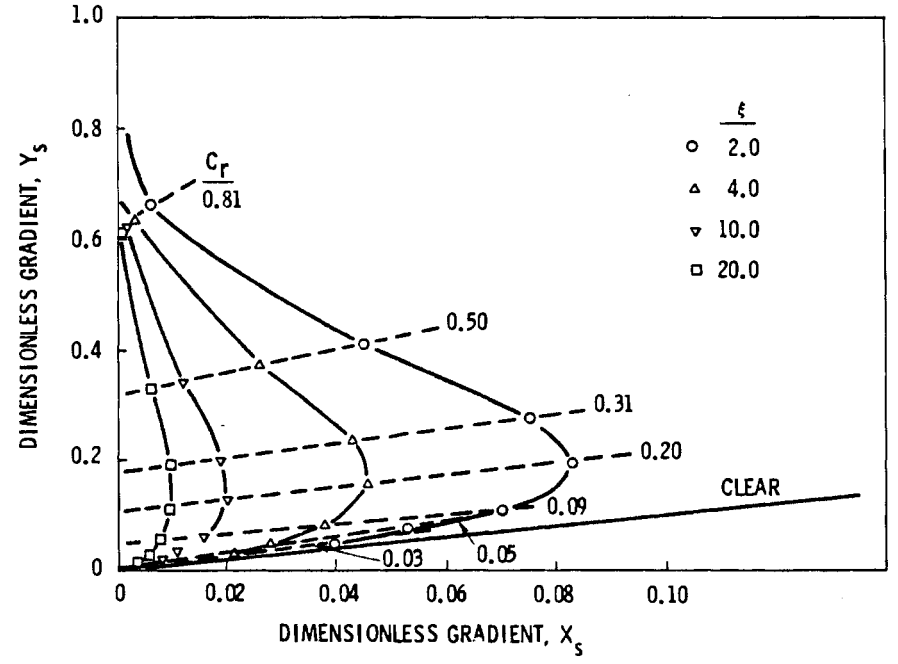

a. Slip-Point Loci

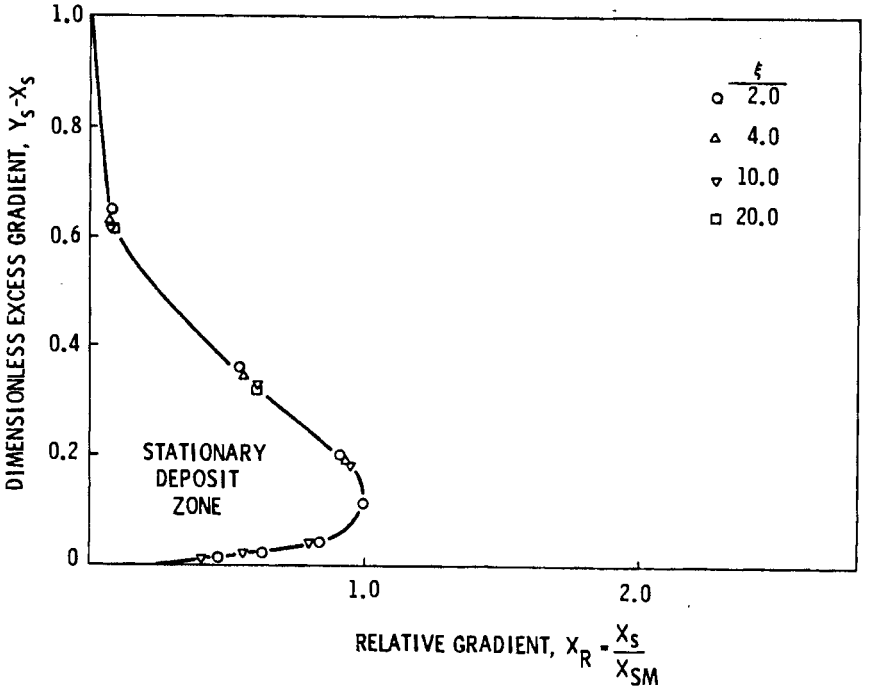

b. Excess Gradient and Stationary Deposit Zone

FIGURE 3.10. Generalized Slip-Point Model

Another aspect, which could be better determined, is the friction factor ratio, ξ, of the proposed model. The method proposed in the original modeling may be sufficient for beds consisting of fairly uniform size. However, for the case in which wide size range or variations in particle shape exist, this parameter may vary.

Another aspect of the proposed slip-point model is the neglect of effect of particle motion at the interface. In a subsequent development, Wilson (1976) extended the slip-point model to account for a bed that effectively slides en masse. In that work, he assumed that the time-averaged effect of saltation on sliding friction at the wall was the same as sliding without saltation. He also accounted for particle motion at the interface by assuming they moved at a velocity equal to the average of the velocity of the fluid above the bed and the velocity of solids in the bed. The possibility of a portion of the solids traveling in suspension in conjunction with a sliding bed was also considered.

In his 1976 paper, Wilson did not actually present the equations he developed. Rather, he presented only a description of the force balance conducted on the sliding bed. In following through the description, keeping in mind the similarity with the slip-point analysis, the equations can be derived as

$$Y = \frac{j}{j_p} = \frac{\phi_1}{(1-a) + \dfrac{a(\phi_2 - C_2 V_R{}^2 \beta)}{\pi - \beta + \phi_2}} \tag{3.35}$$

and

$$X = \frac{j_o}{j_p} = \frac{\left[\phi_1 - (1-a)Y\right]}{\dfrac{\phi_3}{\pi a^2}\left(\phi_2 - C_2 V_R{}^2 \beta\right)}, \tag{3.36}$$

where

$$a = 1 - \frac{\beta - \cos\beta \sin\beta}{\pi}, \tag{3.37a}$$

$$V_R = \frac{V_b}{V_a}, \tag{3.37b}$$

$$\phi_1 = \frac{\sin \beta - \beta \cos \beta}{\pi}, \tag{3.37c}$$

$$\phi_2 = \xi \sin \beta \left[C_1 \left(1 - V_R^2\right)\right], \tag{3.37d}$$

and

$$\phi_3 = \frac{1}{\left[1 + V_R \left(\frac{1-a}{a}\right)\left(1 - C_b\right)\right]^2} . \tag{3.37e}$$

The constants C_1 and C_2 are related to the nature of assumptions made concerning the effectiveness of shear transfer through the moving interface. Using derived values of $C_1 = 1.25$ and $C_2 = 1.0$, the results presented by Wilson (1976) were readily duplicated.

Figure 3.11 shows typical results of the sliding bed model for $\xi = 20$ ($d/D = 0.20$). An interesting aspect of this model is that, at low concentrations ($C_r \leq 0.25$), there seemed to be a discontinuity between the sliding bed model and the slip-point model, as shown in Figure 3.11. At very low concentrations ($C_r = 0.01$), the sliding bed model of Equations (3.35) through (3.37) also shows a deposit locus similar to the slip-point model, but it occurs at lower throughput velocities, i.e., lower X values. It has subsequently been reported (Judge 1979) that the original model developed by Wilson effectively used $C_1 = 1$ and reportedly reduced identically to the slip-point locus given by Equations (3.29) and (3.33) for $V_R = 0$, the stationary bed case. Thus, the discontinuity is a direct consequence of the value of the constant, C_1, which is dependent upon assumptions made about the nature of interfacial shear. The mechanics associated with interfacial motion are especially important in the low velocity region and need to be analyzed in greater detail.

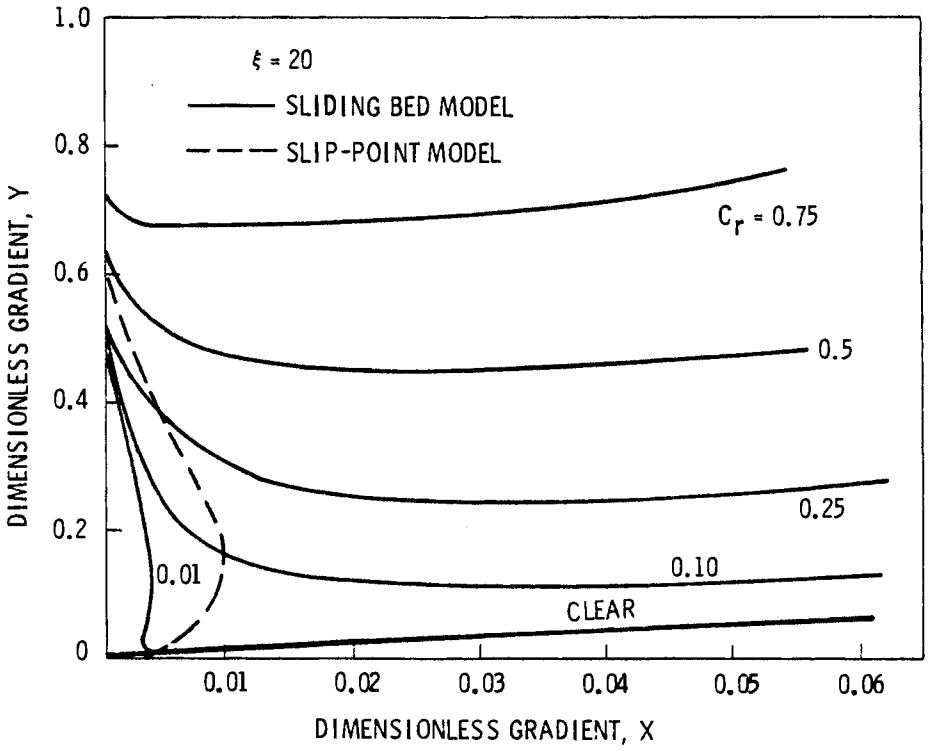

FIGURE 3.11. Concentration Ratio Dependency of the Sliding Bed Model

Another aspect of the model needing improvement is the determination of the fraction of solids being transported in suspension, as it has been found that Equation (3.16) is not generally adequate for particle sizes greater than $d/D \approx 0.03$. For large particle flow it may also be necessary to consider slip flow that may occur through the porous bed material. This throughbed flow would result in an added driving force on the bed material and may affect predictions of the limit of deposition.

Another sliding bed model using a force balance method not totally unlike Wilson's (1976) model was proposed by Pouska and Link (1978) to analyze their oil shale hydrotransport data. To simplify their analysis, they assumed that only two flow regimes existed; 1) a sliding bed where few, if any, saltating particles existed, and 2) a nearly homogeneous suspension. Analysis of the former regime is of particular interest here; a brief description of Pouska and Link's model is presented below.

Considering the case of a single nonspherical particle sliding in a pipe, they derived an expression for the condition in which fluid drag on the particle balanced the mechanical friction on the wall, or

$$\frac{C_D}{\mu_s \chi} = \frac{4}{3} \frac{dg(S - 1)}{(V_a - V_s)^2}. \tag{3.38}$$

The effect of the nonspherical particle is tacitly included as a shape factor χ. If a bed of particles were sliding in the pipe invert, neither C_D nor μ_s could be determined independently. However, by assuming that the same forces that act on the single sliding particle act on the bed of particles, they argued that the ratio on the left-hand side of Equation (3.38) is a constant. The ratio must be determined experimentally by measuring, for example, the maximum liquid velocity, V_a, at the point where the solids bed is just stationary, or $V_s = 0$. They then proposed that the ratio, $C_D/\mu_s\chi$, being a constant, can be used to determine the flow character of the sliding bed.

To determine the pressure drop in the pipe, Pouska and Link then considered the geometry of the bed in the pipe invert and defined an effective relative roughness from which they were able to determine an effective mixture friction factor for the equation

$$\frac{\Delta P}{L} = \frac{f V_a^2 \rho_m}{2D_h}. \tag{3.39}$$

The actual liquid velocity above the bed layer must be used in this expression in conjunction with the appropriate hydraulic diameter, D_h.

After developing this model and comparing predictions with data, Pouska and Link concluded that pressure drop could not be predicted a priori (1978). Bench-scale tests must be performed to determine the ratio $C_D/\mu_s\chi$ and the corresponding bed height to determine the appropriate hydraulic diameter. While this approach may offer advantages over pilot plant testing, it still requires a priori testing.

3.2.3 Data Comparisons

Empirical models lack sufficient generality to be widely applicable to large-particle flow. Mechanistic sliding bed models offer greater potential for performing scale-up calculations even though improvements in certain aspects of current models are needed. In this section, comparisons are made between available data and the slip-point/sliding bed model presented in the previous section.

Although the objective of the hydrotransport plugging project is to investigate large-particle transport, it has become obvious that very little large-particle hydrotransport data are available in open literature. In addition, particular attention to high concentration flow is of concern to this project. A number of flow studies with delivered volumetric concentrations around 40% can be located; however, they generally considered small diameter materials such as sand. Consequently, comparisons made in this section are intended to demonstrate a range of applications of the slip-point/sliding bed model.

In Figures 3.12 and 3.13 oil-shale data of Pouska and Link (1978) are presented.[a] Figure 3.12 shows head loss data for -25 mm x 0 shale pumped in a 208-mm pipe (d/D = 0.06) at a delivered concentration of 6%. The model developed by Pouska and Link (1978), curve E-E in Figure 3.12, shows good agreement with both the observed occurrence of the stationary bed and the hydraulic gradient trend.

For comparison, both the slip-point locus and the sliding bed results of Wilson's model are shown by curves A, B, and C of Figure 3.12. To demonstrate parameter dependency, variations in the coefficient of friction and the assumed effective particle size are shown. The values shown for the coefficient of friction are assumed because they were not reported with the data. The values for ξ of 7.3 and 3.7 correspond to a reported weighted mean diameter of 13 mm and one-fifth that value, respectively. The latter size was recommended by Pouska and Link (1978) as being a more representative value for their model. It is apparent in Figure 3.12 that curve C-C' compares very well with the data.

In Figure 3.13, data for -25 mm x 0 oil shale pumped in a 157-mm line at 14% delivered concentration is compared to the sliding bed model. It is apparent that very good agreement exists between the data and the model in the sliding regime. It is also apparent that, at velocities near the point of the observed stationary bed, the data show a marked decrease in head loss. This is to be expected because, as velocity decreases, delivered concentration also decreases. Thus, although the data in Figure 3.13 may be for a reported concentration of 14%, the in situ concentration would have to be higher and the delivered concentration lower at lower velocities.

While the comparisons shown in Figures 3.12 and 3.13 are very good, it should be noted that other oil shale data presented by Pouska and Link (1978) could not be predicted as well. In general, better agreement could be obtained in the observed sliding bed regime for the -25 mm x 0 shale than for the -4.9 mm x 0 shale. This could be due to several reasons. For the

---

(a) See also Link et al. (1977)

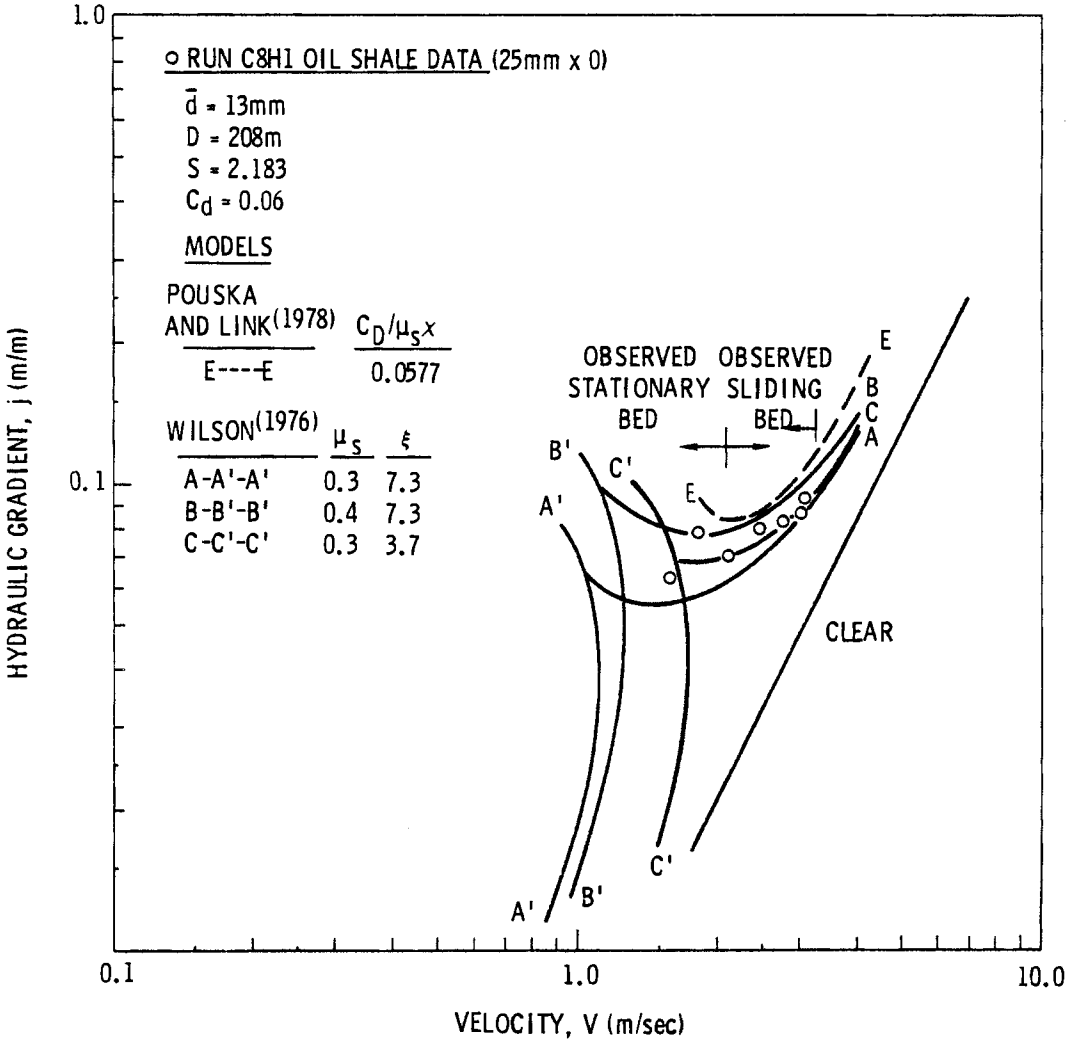

FIGURE 3.12. Comparison of Sliding Bed Model Predictions and Oil Shale Data

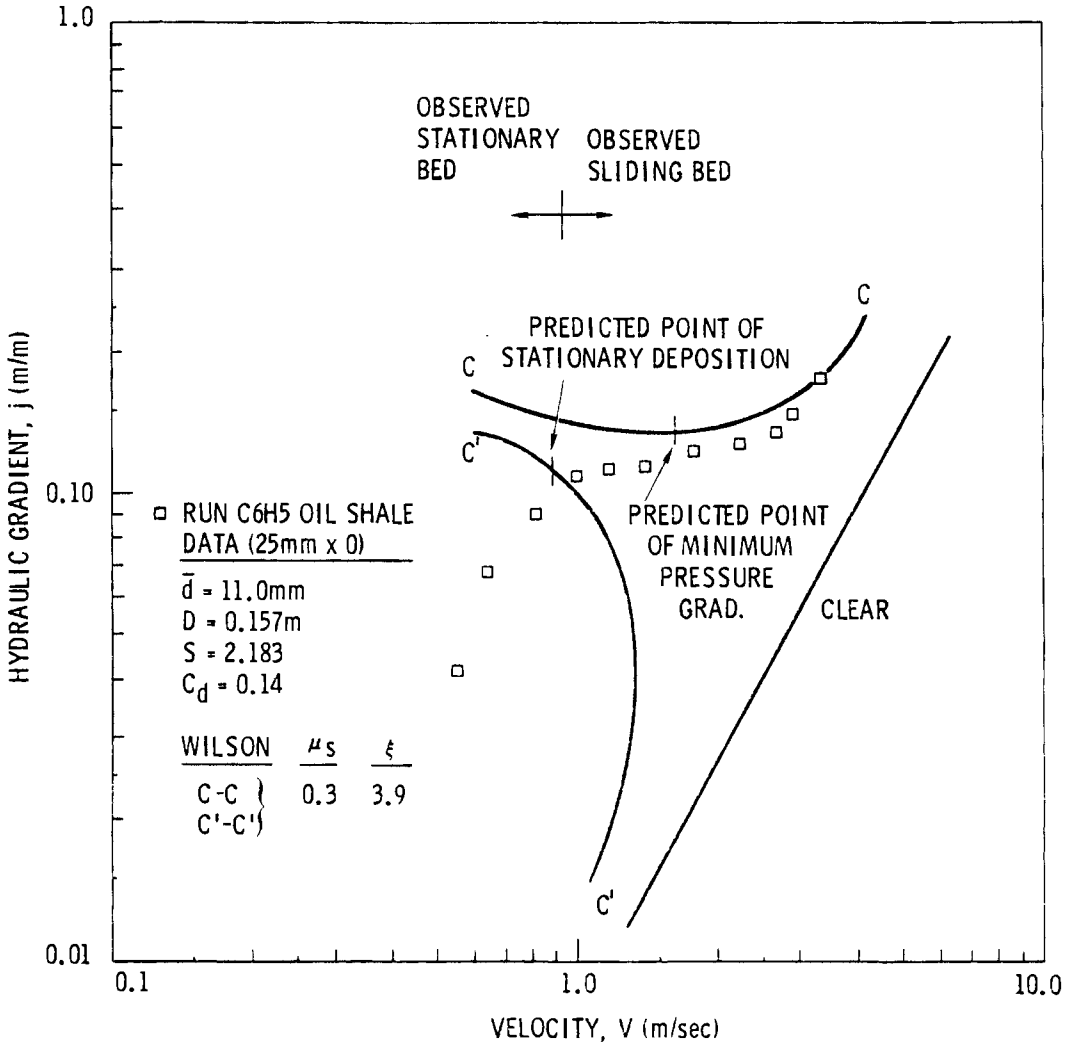

FIGURE 3.13. Comparision of the Predicted Point of Stationary Deposition

smaller-sized shale, a higher percentage of fines was present, which would have some effect, as would the increased fraction of solids in suspension. It has already been noted that estimating the turbulent suspension fraction is one aspect of the model needing improvement.

Carleton et al. (1978) pumped limestone in a 157-mm pipeline at delivered concentrations up to 20% by volume. They also reported that all of their data trends were in reasonable agreement with the sliding bed model of Wilson, although they showed only one comparison. Their narrow size range data are compared with calculations performed in this work in Figure 3.14. The model results calculated at a delivered concentration of 10% are shown by dotted lines. While the trend with particle size is typified, there appears to be significant overprediction of the velocity at which minimum pressure gradient exists. In evaluating the information available in their report it was found that, according to their nomenclature, the results were "interpolated" and at constant in situ concentrations. Therefore, the sliding bed model was re-solved at $C_i = 0.1$, and the results are also shown in Figure 3.14. The agreement between the data and model for the 20- to 40-mm solids is seen to be very good in this case where only sliding bed motion was assumed.(a)

The results shown in Figure 3.14 can also be used to point out two other problems commonly encountered in hydrotransport. One, discussed in a previous section, involves conflicting data trends. Although these data indicate a decrease in head loss in increased size (a trend shown by Wilson's model), Pouska and Link's (1978) oil shale data showed just the oposite trend. Second, and perhaps more significant, it is very difficult to use data gathered and reported in the literature for model comparison. Sufficient understanding of how the data were taken, the nature of the experiment, how solids attrition occurred, and other question are very important. The data reported by Carleton et al. (1978) provides a good example of these points.

(a) A. J. Carleton has since informed the authors that the 1978 paper contained a nomenclature error and the data were purportedly at a constant delivered concentration.

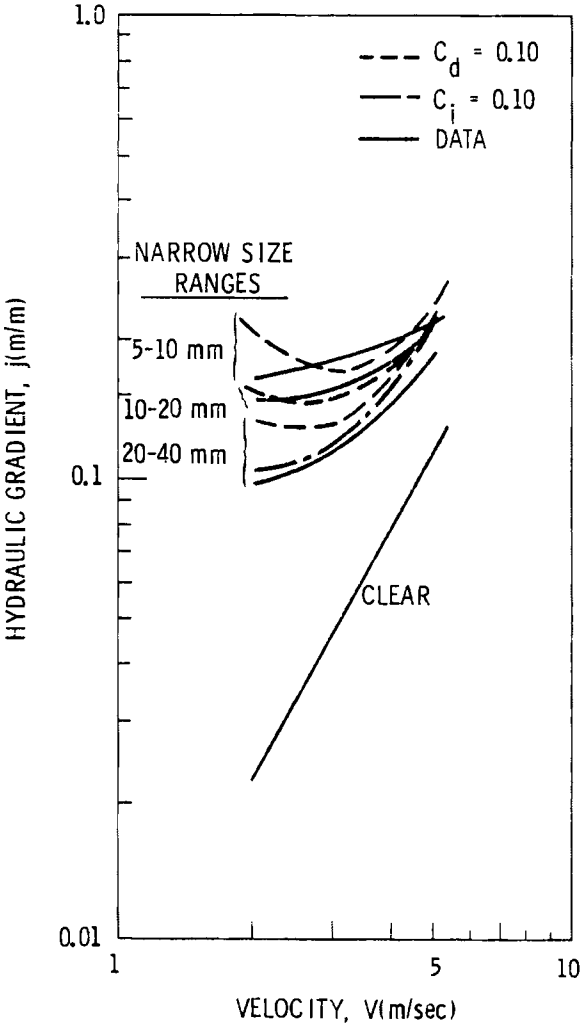

FIGURE 3.14. Predicted Hydraulic Gradient for Limestone Transport

Wang and Seman (1973) measured primary variables in a well-controlled experiment to determine the effect of pipe shape geometry on head loss. They used relatively small glass bead particles (14 x 16 U.S. mesh, $\bar{d}$ = 1.379 mm) and measured delivered concentrations up to 15.5%. Comparisons of their data with Wilson's sliding bed model show another example of the versatility of the model.

As shown in Figure 3.15, using the assumption that the glass beads move as a sliding bed, the model tends to overpredict the head loss at C_d = 15.5%, but follows the low concentration data fairly well in the circular pipe geometry. The overprediction at the higher concentration is to be expected since no suspension was included in these predictions. In Figures 3.16 and 3.17, similar comparisons are made for the rectangular pipe geometries with the long side oriented horizontally and vertically, respectively.

In the original work, Wang and Seman (1973) reported results of delivered concentration versus velocity for each of the geometries tested. From these curves it was determined that, above an apparent mean velocity of approximately 1.5 m/sec, delivered concentration was relatively invariant with velocity increase. At lower velocities delivered concentration decreased significantly with a decrease in velocity. It is interesting to note that in Figures 3.16 and 3.17, for a velocity above 1.5 m/sec, the head loss difference between the predicted and measured solids flow is approximately a constant. On a linear scale, this constant logarithmic difference would be an exponentially increasing function. This observation is in agreement with assumptions made in the sliding bed model when turbulent suspension is included. When turbulent suspension is included through an equation such as (3.7) it is assumed (Wilson 1976) that the fraction of solids traveling in a sliding bed mode is given by

$$\frac{C_c}{C_d} = \left(\frac{V_t}{V}\right)^2 . \tag{3.40}$$

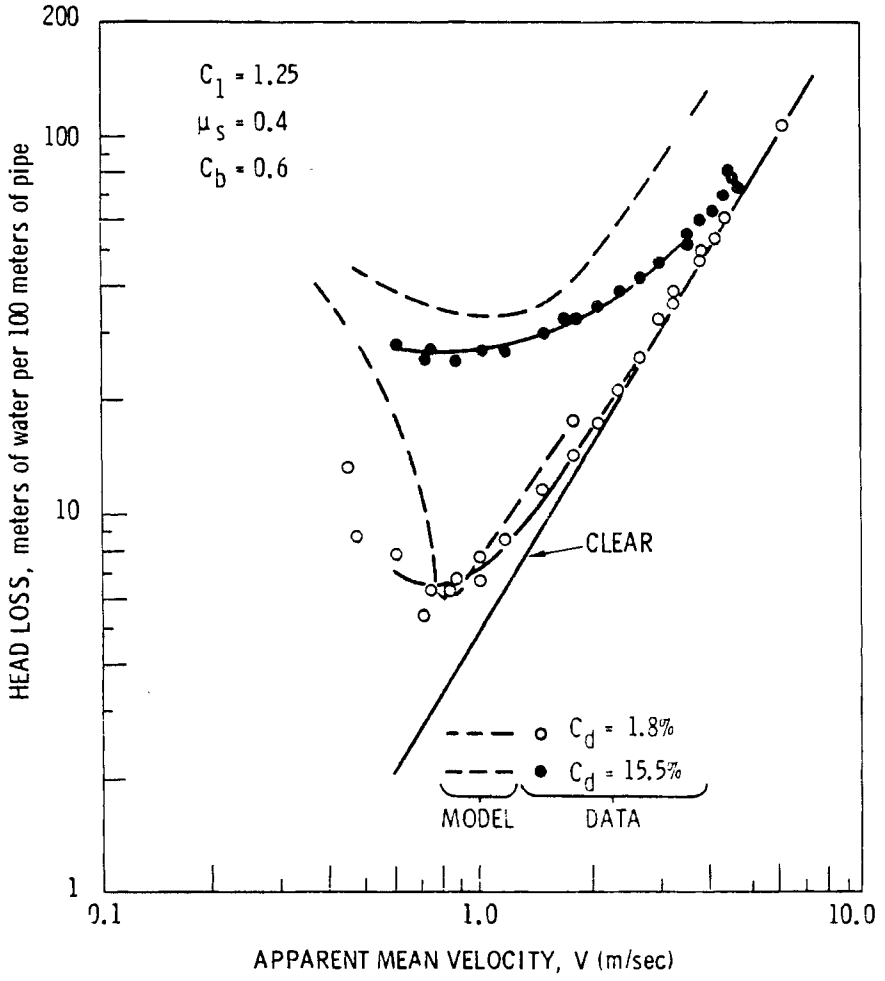

FIGURE 3.15. Predicted Hydraulic Gradient for Uniform Glass Beads in a 1-in. Pipe

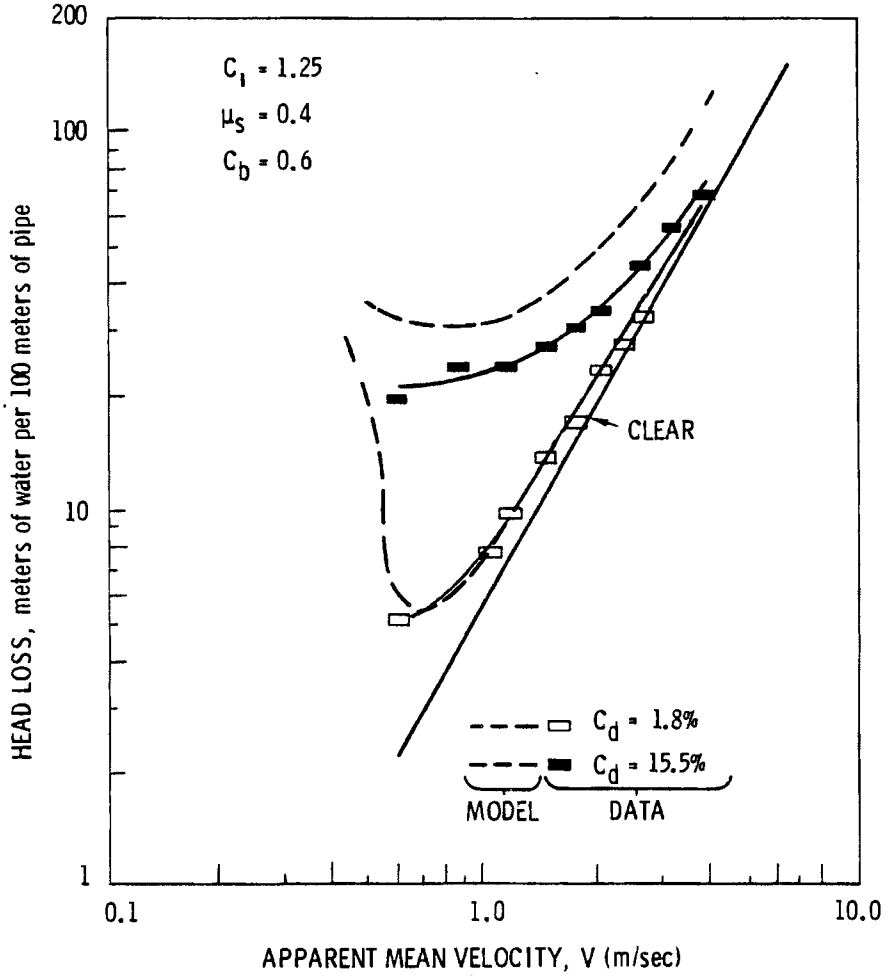

FIGURE 3.16. Predicted Hydraulic Gradient for Uniform Glass Beads in a Rectangular Pipe for H/W = 0.5

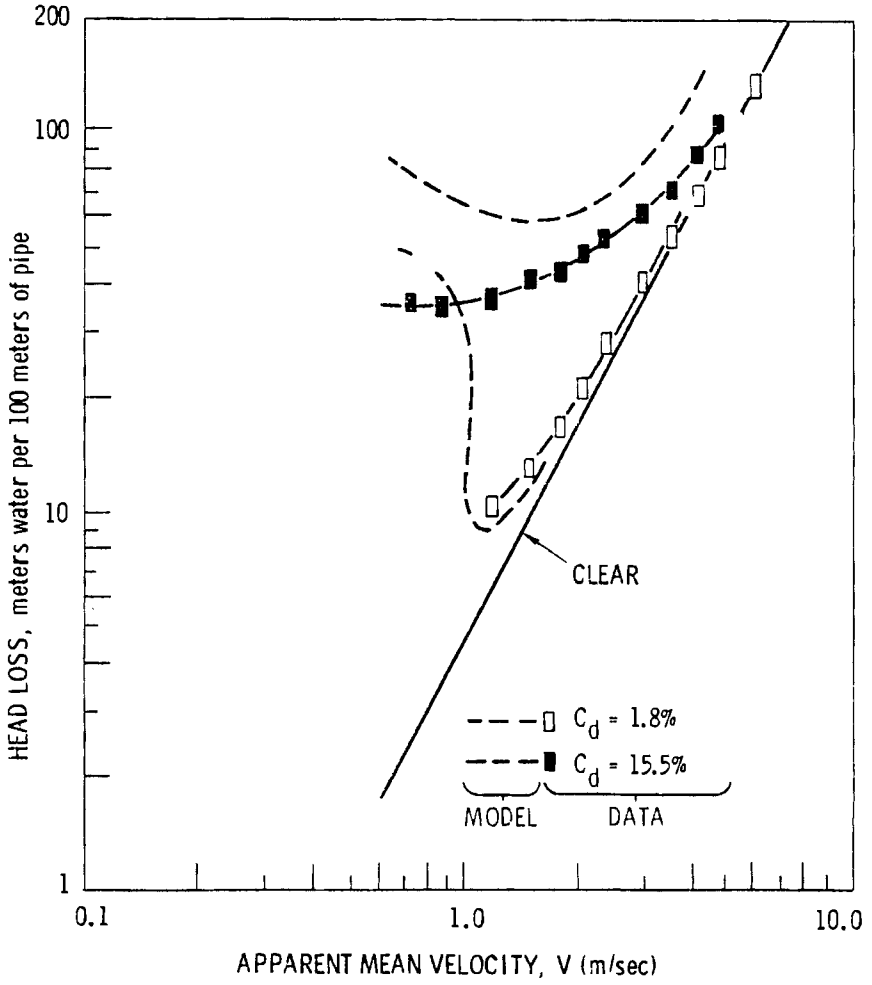

FIGURE 3.17. Predicted Hydraulic Gradient for Uniform Glass Beads in a Rectangular Pipe for H/W = 2.0

where C_c is the concentration of solids traveling as contact load, i.e., in a sliding bed. Thus, for velocities above the turbulent suspension velocity, V_t, the contact load fraction would be exponentially decreasing and the predicted headloss, assuming all sliding bed motion at all velocities, would appear as a constant logarithmic difference over measured headloss.

The data for the rectangular channels indicate this result, but the data for the circular pipe do not. This may be directly due to geometry. For the rectangular shapes, the interfacial area between the carrier fluid and the solids bed is effectively independent of velocity. On the other hand, in the circular pipe, as velocity varies, the amount of settled material varies. This leads directly to variations in interfacial area. It can further be argued that the mechanisms associated with turbulent suspension can be related to the interfacial area over which solids can be picked up and redeposited. It has been previously mentioned that the modeling of interfacial shear in the mechanistic sliding bed model must be further investigated. The above argument and Wang and Seman's data offer further support for that contention.

Results presented in this section support the conclusion that the force balance mechanistic model provides the greatest potential for predicting plugging and operational characteristics in a large particle hydrotransport pipeline. Earlier empirical and regression curve-fit models were shown to predict widely varying plugging velocities for given flow conditions. They cannot be extrapolated with confidence, as they can treat only a single characteristic particle size or limited parameter ranges. The force balance approach treats the flow mechanistically, accounting for wall friction, interfacial shear, and suspension load in conjunction with sliding bed load. It treats particles of different sizes by segmenting a distribution into discrete sizes and predicting the cumulative effect.

While the mechanistic modeling approach in its current state offers the greatest potential for scale-up calculations, several aspects of the modeling process need to be refined or improved. The equivalent roughness approach to modeling interfacial shear requires further investigation. Throughbed flow,

which was not included, may be of significant concern to large particle plugging. These and other aspects form the basis for continued analytical work to be conducted in this study.

4.0 ANALYTICAL MODELING

The conclusions reached in Task 1 provided guidance and direction for the work being conducted in this task. The primary goal of Task 2 is to develop improvements to the modeling predictions of the occurrence of plugging or limit of stationary deposition. Of principal concern is the application of these models to large particle, run-of-mine hydrotransport.

To improve model capabilities, analytical efforts are to be directed toward describing the effect of throughbed flow, interfacial shear, turbulent suspension, and particle size distribution within the framework of the force balance, sliding bed approach. In addition, attention will be directed toward developing a two-solid, stratified bed model, which will have application to run-of-mine operation where a potential for mixtures of rock and coal may be present.

Work on this task is currently in progress. In this section, discussions are presented for work that has been completed. In the areas where no work has yet commenced, only a brief review of the tentative direction is given.

4.1 SINGLE-SOLID MODEL IMPROVEMENTS

The areas that were identified as requiring improvements or enhancements to the modeling of the limit of stationary deposition for single-solid flow include the effects of throughbed flow, interfacial shear, turbulent suspension, and particle size distribtuion. These areas are to be approached in this task. The direction and anticipated accomplishments are discussed below.

4.1.1 Throughbed Flow

In the original development of the force balance model of single-solid bed flow discussed in Section 3.2, the only account made for carrier fluid flow within a sliding bed of solids was in the resistance to flow caused by the fluid friction between the moving bed layer and the pipe wall. This effect was modeled simply through an added clear water friction factor for *in situ*

fluid flowing in the bed region at the same velocity as the sliding bed. This effect was not included in the limit of stationary deposition model.

Although no detailed analysis has yet been performed, there are several potential methods to treat the effect of throughbed flow. This flow would give rise to an additional driving force acting on the bed due to the relative velocity difference between the carrier fluid and the solids. Conversely, additional drag is experienced by the fluid, causing a further increase in pressure drop. Therefore, one alternative may be to use a modified drag coefficient to describe flow resistance. It is envisioned that this approach could be used directly in conjunction with the model developed in Section 3.2.2 through direct determination of an additional "body" force on the bed material acting in the direction of flow.

Another alternative would be to treat the bed material as a porous medium. In this manner, flow through the bed could be described as proportional to porosity or void fraction. The difficulty of this approach may be in determining an appropriate resistance coefficient as commonly used in porous media flow (Scheidegger 1960). Independent of the modeling approach, the anticipated overall effect of the throughbed flow should serve to lower flow velocity at which stationary deposition limits are predicted.

4.1.2 Interfacial Shear

In the current modeling approach, interfacial shear is determined based on an effective friction factor as discussed in Section 3.2.2. The shear is modeled as

$$\tau_i = f_i \rho \frac{V_a^2}{8} \tag{4.1}$$

with the interfacial friction factor being determined from Nikuradse's formula as

$$f_i = 2f = 2\left[2 \log_{10}\left(\frac{D}{d}\right) + 1.14\right]^{-2}. \tag{4.2}$$

In Equation (4.2), the equivalent sand grain roughness normally used has been replaced by the particle diameter, d. Typical values that result for f_i range from 2 to 20 times clear water values for particle-to-pipe diameter ratios up to 0.20.

The assumption that f_i is twice Nikaradse's friction factor was originally proposed by Wilson (1976), although justification for the factor of 2 was not well-supported. Since interfacial shear is a contributor to a driving force on a bed, further support of this or an alternative approach needs to be found. This is an intent of experimental work to be conducted under Task 3 of this project.

4.1.3 Turbulent Suspension

As discussed in Section 3.1.3, the criterion proposed by Wilson and Watt (1974), and used in conjunction with the sliding bed model to determine suspended fractions, was not wholly adequate for large particle-to-pipe diameter ratios. It is not the intention of this work to develop a new model. Rather, an effort will be made to review transport literature and compare various models. It is anticipated that such a review will provide better insight into the support mechanisms and perhaps yield a better model than is currently available.

4.1.4 Particle Size Distribution

In a run-of-mine operation, detailed knowlege of size distribtuion cannot be expected a priori. Thus, even with the recognition that description of the solids by a single characteristic size is not wholly adequate, it may prove to be sufficient, in light of the uncertainties associated with a variation in distribution with time. Based on this argument, this task will undertake to determine the effect a size distribution variation would have on steady-state operating conditions.

The anticipated approach to be taken involves the use of the slip-point/sliding bed model developed in Section 3.2.2. The fraction weighted average size given by Equation (3.3) and the individually treated segmented method proposed by Wilson (1976) in conjunction with his sliding

model will be used. They will be used to parameterize the predicted point of plugging for probabalistic type variations about a known size distribution. It is currently felt that this approach will result in an estimation of the sensitivity of prediction with size distribution variations.

4.2 TWO-SOLID STRATIFIED MODEL

During operation of a mine transport system, there is a potential for a solids mixture of rock and coal to coexist in the pipeline. Depending upon the throughput velocity and relative concentrations, the flow regime may be characteristic of a single solid if the velocity is sufficiently high to produce a fully suspended or pseudohomogeneous flow. At lower velocities, it seems readily envisionable that a sliding bed type of flow may be characteristic. In this event, a stratified bed flow may occur at the lower velocities if the solids present have significantly different specific gravities. At intermediate velocities, there is the conceptual possibility that the lighter solid may be saltating or suspended while the heavier material is in a sliding bed mode.

The expectation of these flow regimes is based on phenomena observed and reported for single-solid flow. No two-solid visualization experiments that support the contended flow regimes are known to exist. Drawing on the experience of the force balance analysis conducted for single-solid tranport will allow the development of a two-solid, stratified, bed-flow model. In this section, work accomplished toward that development is presented. The goal is to provide the basic model that can be used to predict the limit of stationary deposition for run-of-mine application and upon which further development may be based to improve those predictions.

The basic geometry used in developing this model is shown in Figure 4.1. The flow model assumes the existence of stratified solids with specific gravities S_1 and S_2 in the pipe invert. Carrier fluid flows in the region above the solids.

As in the single-solid model, the driving forces on the bed load are consequences of the pressure gradient and interfacial shear between the carrier

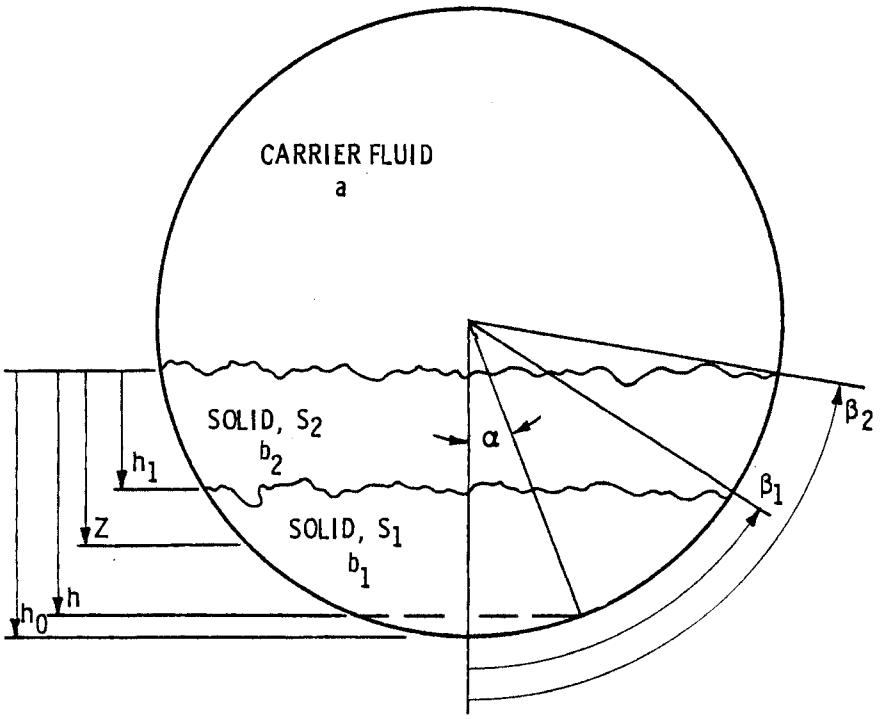

FIGURE 4.1. Stratified Two-Solid Flow Model

fluid and the top layer of solids. Resisting forces are due to friction between the solids and the pipe wall, and the viscous resistance of the fluids. The two-solid model reduces to the single-solid model (compare Figure 4.1 with Figure 3.9) as the in situ concentration of either solid goes to zero. Similarly, as the pipe fills up, the single solid plug flow must be encountered in the absence of one or the other solid. These limits will be useful in the subsequent development.

4.2.1 Plug Flow Gradient

Determination of the plug flow gradient in the single-solid model proved useful as a generalized normalization factor. At this point, it is assumed that it should be as useful in the two-solid model.

In deriving the plug flow gradient, it was assumed that the intergranular pressure in the solids can be described as a hydrostatic distribution of the solids' submerged weight. The hydrostatic pressure distribution, P_s, can be expressed as

$$\frac{dP_s}{dz} = (\rho_s - \rho)\, g C_b. \tag{4.3}$$

In terms of specific gravity, this can be rewritten as

$$\frac{dP_s}{dz} = \rho g C_b\, [S(z) - 1], \tag{4.4}$$

where $S(z)$, the specific gravity, is a function of vertical position. This implies that no inhomogeneity of the solids exists across a horizontal plane. Vertical inhomogeneity due to stratified solids is accounted for.

Using the carrier fluid-solid interface as a datum, the pressure distribution can be determined if the specific gravity is known or assumed constant for each solid. At this point, integration of Equation (4.4) for $z < h_1$ (see Figure 4.1) yields[(a)]

(a) Circled superscripts refer to the two-solid stratified model.

$$P_s^{(2)} = \frac{C_b D\rho g}{2} (S_2 - 1) (\cos \alpha - \cos \beta_2) \tag{4.5}$$

for the upper solid region for $\beta_1 < \alpha < \beta_2$. In the lower region for $h_1 < z < h_o$, integration yields

$$P_s^{(2)} = \frac{D\rho g}{2} \left[(S_2 - 1)C_{b2}(\cos \beta_1 - \beta_2) + (S_1 - 1)C_{b1}(\cos \alpha - \cos \beta_1)\right]$$

for $0 < \alpha < \beta_1$. (4.6)

The normal force exerted by the solids on the wall, which is required to determine the resistance of the bed due to friction on the wall, is given by

$$F_N^{(2)} = D \int_o^{\beta_2} P_s^{(2)}(\alpha)\, d\alpha \quad . \tag{4.7}$$

This equation can be integrated to yield

$$F_N^{(2)} = \frac{\pi D^2}{2} \rho g \left\{(S_2 - 1)\, C_{b2} \left(\frac{\sin \beta_2 - \beta_2 \cos \beta_2}{\pi} - \frac{\sin \beta_1 - \beta_1 \cos \beta_1}{\pi}\right) + (S_1 - 1)\, C_{b1} \left(\frac{\sin \beta_1 - \beta_1 \cos \beta_1}{\pi}\right)\right\} . \tag{4.8}$$

In this expression, the packed bed fractions, C_{b1} and C_{b2}, have been included separately for generality. For the limits of $\beta_1 \to 0$, $\beta_1 \to \beta_2$, and $\beta_2 \to \beta_1$, Equation (4.8) reduces to the single-solid result

$$F_N = \frac{\pi D^2}{2} \rho g \left\{C_b(S-1) \frac{(\sin \beta - \beta \cos \beta)}{\pi}\right\} . \tag{4.9}$$

In addition to the pipe diameter and carrier fluid density, the normal force is a function of the packed bed fractions, specific gravities, and relative concentration expressed through the angles, β_1 and β_2. This is expressed in functional form as

$$F_N^{(2)} \alpha f_N^{(2)} (C_{b1}, C_{b2}, S_1, S_2, \beta_1, \beta_2). \tag{4.10}$$

The submerged weight, $W_N^{(2)}$, of the two-solid bed must be considered. From the basic principle of buoyancy the submerged weight can be expressed as

$$W_N^{(2)} = \frac{\pi D^2}{4} \rho g \left\{ C_{b1} (S_1 - 1) \left(\frac{\beta_1 - \cos \beta_1 \sin \beta_1}{\pi} \right) \right.$$

$$\left. + C_{b2} (S_2 - 1) \left(\frac{\beta_2 - \cos \beta_2 \sin \beta_2}{\pi} - \frac{\beta_1 - \cos \beta_1 \sin \beta_1}{\pi} \right) \right\} \tag{4.11}$$

or, in functional form,

$$W_N^{(2)} \alpha w_N^{(2)} (C_{b1}, C_{b2}, S_1, S_2, \beta_1, \beta_2) \quad . \tag{4.12}$$

It can be readily shown that this expression reduces to the single-bed expression

$$W_N = \frac{\pi D^2}{4} \rho g \, C_b \, (S - 1) \left(\frac{\beta - \cos \beta \sin \beta}{\pi} \right) \quad . \tag{4.13}$$

The ratio of the normal force to the submerged weight thus becomes

$$\frac{F_N^{(2)}}{W_N^{(2)}} = \frac{2 \cdot f_N^{(2)} (C_{b1}, C_{b2}, S_1, S_2, \beta_1, \beta_2)}{w_N^{(2)} (C_{b1}, C_{b2}, S_1, S_2, \beta_1, \beta_2)} \quad . \tag{4.14}$$

To demonstrate the nature of the ratio, Equation (4.14) is plotted in Figure 4.2 for $C_{b1} = C_{b2} = 0.6$. A complex family of curves as a function of β_1 and β_2 is shown.

Several interesting observations are notable in Figure 4.2. For both the single-solid model, $\beta < 90^\circ$, and the double-solid model, $\beta_1 < \beta_2 < 90^\circ$, there is little difference between submerged weight and normal force. Additionally, there is an asymmetric nature to the two-solid ratio about the single-solid line at larger angles. This is also apparent in Figure 4.3 where the ratio is shown for a full pipe ($\beta_2 = 180^\circ$) as a function of β_1. The limits at $\beta_1 = 0$ and 180° show the single-solid result of $F_N/W_N = 2$, but, at other angles, a stratified bed exhibits varying behavior.

The plug flow gradient can be determined from a force balance by equating the force due to pressure gradient at the point of slip to the friction force, $\mu_s F_N^{(2)}$, or

$$\rho g j_p^{(2)} \frac{\pi D^2}{4} = \mu_s F_N^{(2)}$$

$$= \mu_s \rho g \frac{\pi D^2}{2} f_N^{(2)} (C_{b1}, C_{b2}, S_1, S_2, \beta_1', \beta_2 = 180^\circ) \quad . \qquad (4.15)$$

For known or assumed solids properties, the plug flow gradient becomes a function of the relative concentration expressed through the angle β_1' for $\beta_2 = 180^\circ$, or

$$j_p^{(2)} = 2 \mu_s f_N^{(2)} (\beta_1', \beta_2 = 180^\circ). \qquad (4.16)$$

The functional form of $f_N^{(2)}$ is given by the term in brackets $\{\}$ in Equation (4.8). For equal packed bed fractions and known specific gravities, it can be expressed as

$$j_p^{(2)} = 2 \mu_s C_b \left[(S_2 - 1) (1 - f_1) + (S_1 - 1) f_1 \right], \qquad (4.17)$$

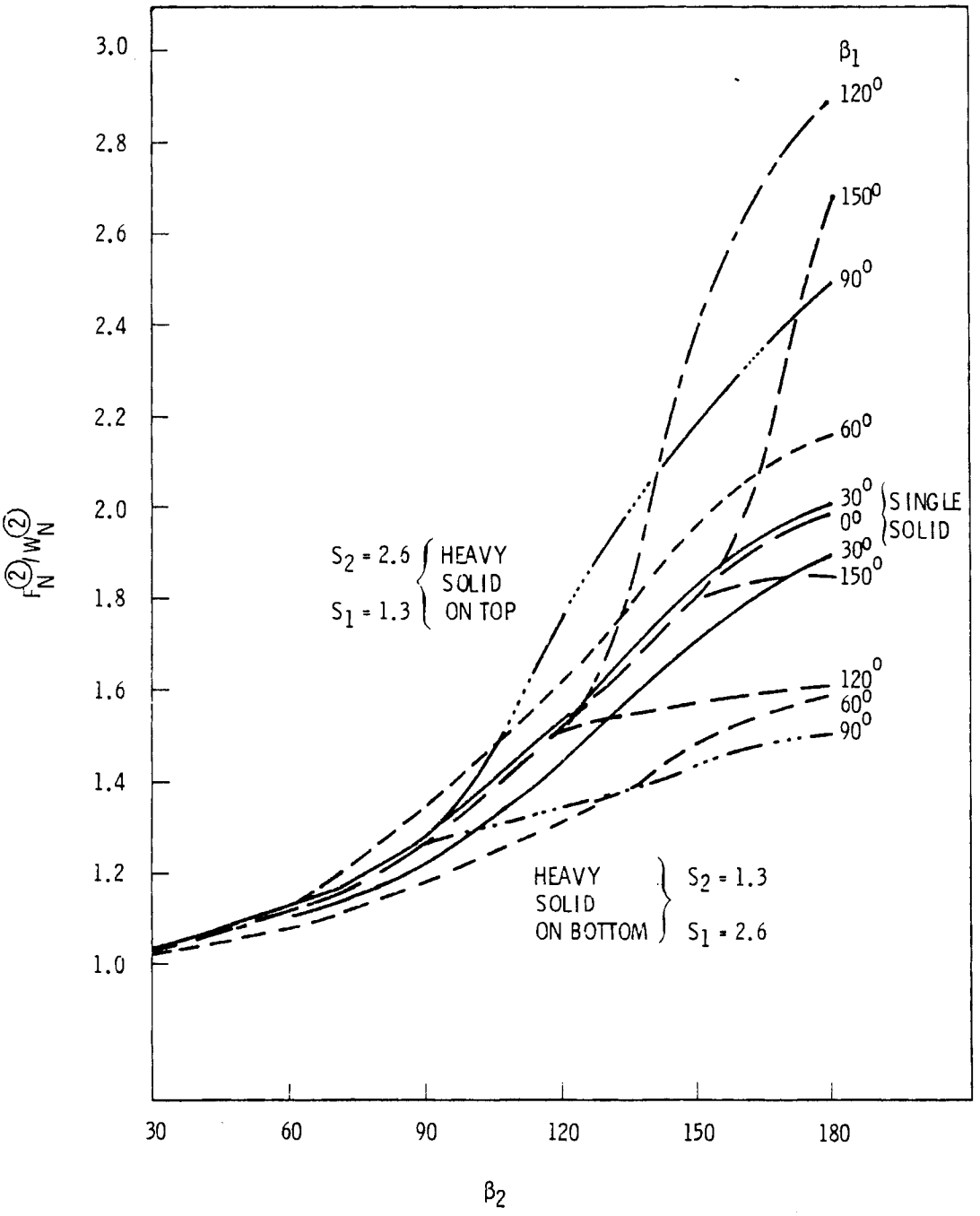

FIGURE 4.2. Bed-Angle Dependence of $F_N^{(2)}/W_N^{(2)}$ on β_1 and β_2

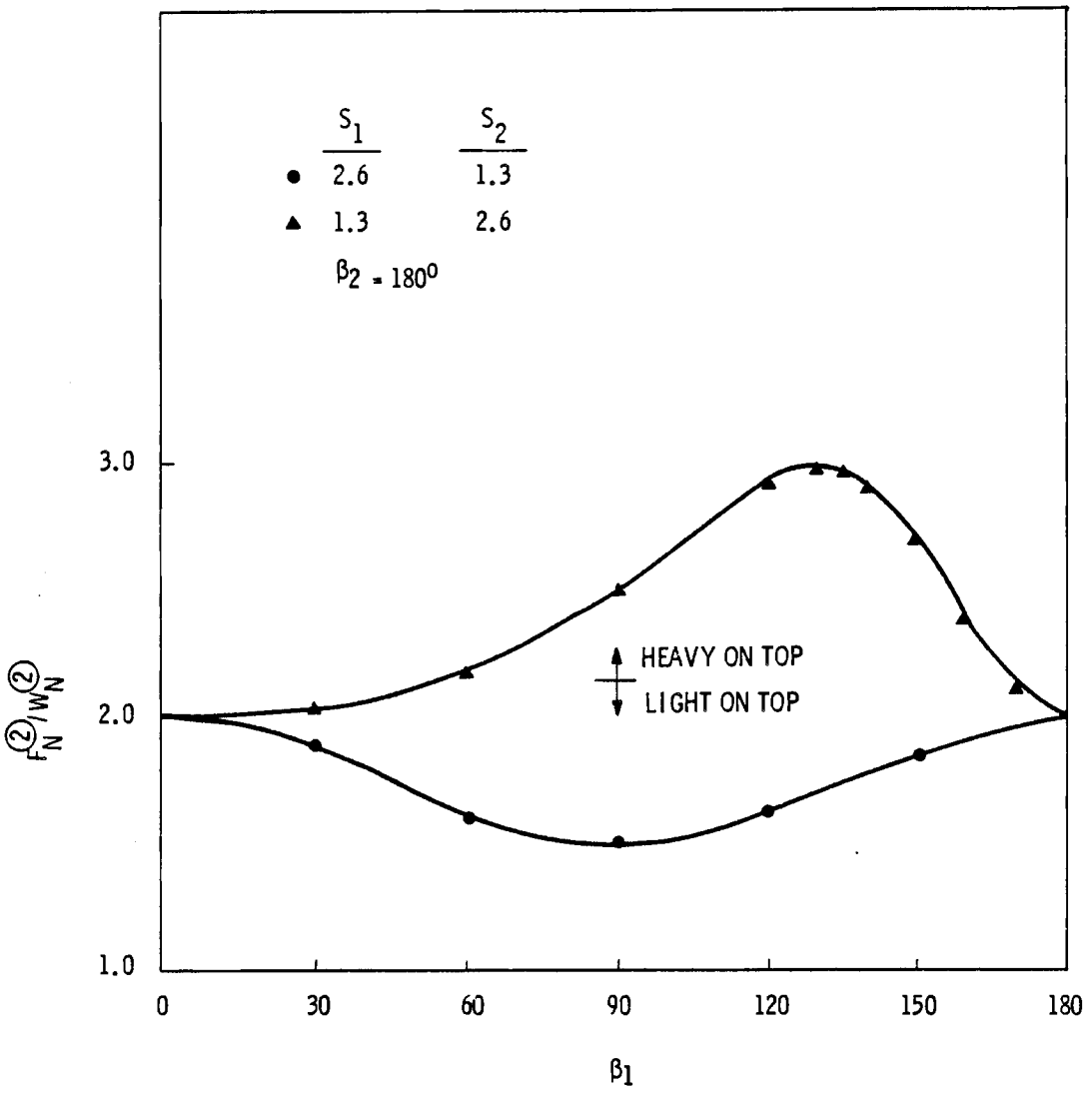

FIGURE 4.3. Bed-Angle Dependence of $F^{②}_{N}/W^{②}_{N}$ on β_1 at $\beta_2 = 180^{\circ}$

where, for convenience, the dimensionless fraction is defined as

$$f_1 = \frac{\sin \beta_1' - \beta_1' \cos \beta_1'}{\pi} \tag{4.18}$$

A typical plug flow gradient based on Equation (4.17) is shown in Figure 4.4. It is apparent from the figure that the gradient is a nonlinear function of the relative concentration of solids. Note that the single-solid results are approached at $\beta_1 = 0^\circ$ and $\beta_1 = 180^\circ$ as predicted by Equation (3.20)

One question arising from this plug flow gradient derivation is whether it will serve as a generalized normalization factor for the two-solid model as it did for the single-solid model. Although this question has not yet been fully resolved, there does not seem to be any a priori reason as to why it should not work in a similar manner. Work is currently being conducted to rationalize whether equivalent volume fraction ratios, weight fraction ratios, or perimeter ratios are most appropriate for determining equivalent plug flow gradients.

4.2.2 Limit of Deposition

The limit of stationary deposition can be derived following the same basic procedure used in the single-solid model. Initially, it is assumed that the coefficient of friction, μ_s, is constant and the same for both solids. This allows the resisting force on the bed in the pipe to be written as

$$F_{R,b}^{(2)} = \mu_s F_N^{(2)}$$

$$= \mu_s \frac{\pi D^{(2)}}{2} \rho g f_N^{(2)} \left(C_{b1}, C_{b2}, S_1, S_2, \beta_1, \beta_2 \right) . \tag{4.19}$$

Using the plug flow gradient given by Equation (4.17), Equation (4.19) can be written as

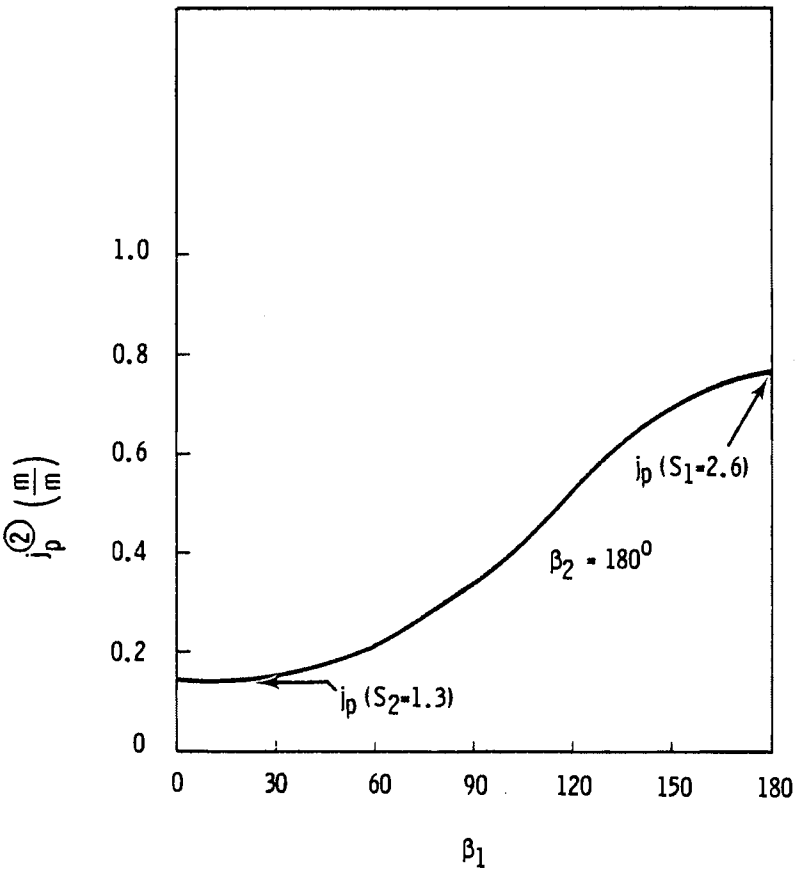

FIGURE 4.4. Plug Flow Gradient for Two-Solid Stratified Model

$$F_{R,b}^{②} = \rho g \, j_p^{②} \frac{\pi D^2}{4} \frac{f_N^{②}(\beta_1, \beta_2)}{f_N^{②}(\beta_1', \beta_2 = 180^\circ)}, \tag{4.20}$$

where, for clarity, the packed bed fractions and specific gravities have been omitted from the argument lists. According to the discussion on plug flow gradient, the angle β_1' has not yet been defined.

At this point it is convenient to note (see Figure 4.1) that the sum of the area fractions must equal unity, or

$$a + b_1 + b_2 = 1, \tag{4.21}$$

where

$$a = 1 - \frac{\beta_2 - \cos \beta_2 \sin \beta_2}{\pi} = a(\beta_2), \tag{4.22}$$

$$b_1 = \frac{\beta_1 - \cos \beta_1 \sin \beta_1}{\pi} = b(\beta_1) \tag{4.23}$$

and thus

$$b_2 = 1 - a - b_1 = b_2(\beta_1, \beta_2). \tag{4.24}$$

The driving forces on the bed include those due to pressure gradient and relative slip at the interface or interfacial shear. For this initial development, it is assumed that the two solids move as a single bed, which is in line with the constant μ_s assumption. These assumptions will be relaxed at a later point in the development.

The two driving forces due to pressure gradient and interfacial shear are additive and can be expressed as

$$F_D^{(2)} = \rho g j \frac{\pi D^2}{2} \left\{ [1 - a(\beta_2)] + \tau_i D \sin \beta_2 \right\}. \tag{4.25}$$

Accordingly, the current modeling approach to the interfacial shear is to let

$$\tau_i = \xi \tau_o \tag{4.26}$$

where τ_o is an equivalent clear water term determined as

$$\tau_o = f_o \frac{\rho V_a^2}{8}. \tag{4.27}$$

For the fluid layer, the driving and resisting forces are equated and rearranged to yield

$$\tau_o D = \frac{\rho g j \frac{\pi D^2}{4} a(\beta_2)}{\pi - \beta_2 + \xi \sin \beta_2}. \tag{4.28}$$

Equations (4.26) and (4.28) can be substituted back into Equation (4.25) and then equated to the resisting force in Equation (4.20). After rearranging, the slip-point gradient for the two-solid model becomes

$$Y_s^{(2)} = \frac{j_s^{(2)}}{j_p^{(2)}} = \left[\frac{f_N^{(2)}(\beta_1, \beta_2)}{f_N^{(2)}(\beta_1', \beta_2 = 180^\circ)} \right] \left[[1 - a(\beta_2)] + \frac{a(\beta_2)\ \xi \sin \beta_2}{\pi - \beta_2 + \xi \sin \beta_2} \right]^{-1} \tag{4.29}$$

This equation corresponds to Equation (3.29) derived for the single-solid model. The only difference is the added complexity of the first term on the right-hand side and its dependence on the relative solid fractions through the bed angle β_1.

As previously mentioned, the angle β_1' has yet to be determined. How it is determined depends upon the nature of the assumption made to determine plug flow gradient. One method of determining β_1' would be to assumed that *in situ* concentrations in the filled pipe are equivalent to those for sliding bed flow. This is shown graphically in Figure 4.5, in which it is assumed that

$$\frac{b_1}{b_2} = \frac{b_1'}{b_2'} \tag{4.30}$$

Substituting the definitions of Equations (4.23) and (4.24) into (4.30) results in a need to solve the expression

$$\beta_1' - \cos \beta_1' \sin \beta_1' = \pi \frac{b_1}{b_2} \tag{4.31}$$

for the corresponding angle β_1'. This must be done iteratively, as β_1' cannot be solved for explicitly.

To determine β_1' from Equation (4.31), b_1 and b_2, the area fractions of each solid, must be known. Note that the area fractions and the volume fractions per unit length are relatable as

$$b_1 = \frac{q_{s1} C_v}{C_{b1}} = \frac{C_{s1}}{C_{b1}} = \frac{\beta_1 - \cos \beta_1 \sin \beta_1}{\pi} \tag{4.32}$$

and

$$b_2 = \frac{q_{s2} C_v}{C_{b2}} = \frac{C_{s2}}{C_{b2}} = \frac{\beta_2 - \cos \beta_2 \sin \beta_2}{\pi} - b_1. \tag{4.33}$$

Thus, either the relative ratio of solids by volume, q_{s1} and q_{s2}, and the total concentration, C_v, must be specified, or the individual concentrations, C_{s1} and C_{s2}, must be specified where

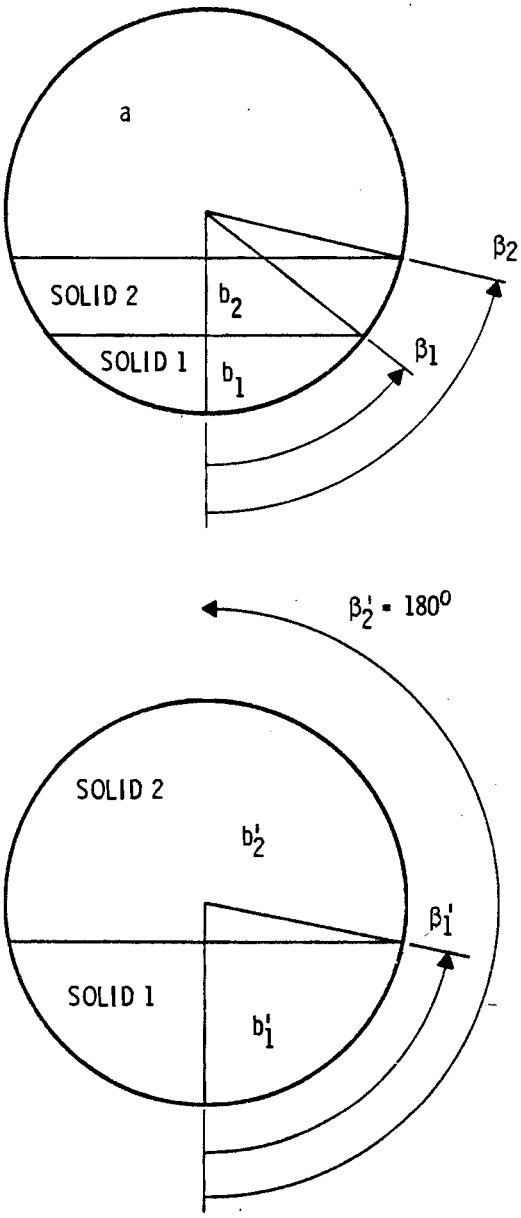

FIGURE 4.5. Representation of Equivalent Solids Fractions for Plug Flow Gradient

$$q_{si} = \frac{v_{si}}{v_s}, \tag{4.34}$$

$$C_v = \frac{v_s}{v_T}, \tag{4.34}$$

and

$$C_{si} = \frac{v_{si}}{v_T} = q_{si} C_v. \tag{4.36}$$

It should, be noted that, accordingly, the following relations must hold:

$$q_{s1} + q_{s2} = 1 \tag{4.37}$$

and

$$C_{s1} + C_{s2} = C_v. \tag{4.38}$$

Similarly, weight fractions may also be used through the following relationships:

$$C_{s1} = \frac{v_{s1}}{v_T}$$

$$= \frac{C_{w1}}{S_1 - (S_1 - 1)C_{w1} - \frac{S_1}{S_2}(S_2 - 1)C_{w2}} \tag{4.39}$$

$$C_{s2} = \frac{v_{s2}}{v_T}$$

$$= \frac{C_{w2}}{S_2 - (S_2 - 1)C_{w2} - \frac{S_2}{S_1}(S_1 - 1)C_{w1}} \tag{4.40}$$

Equations (4.39) and (4.40) result from a simultaneous solution of the general expression

$$C_{wi} = \frac{S_i C_{vi}}{1 + \sum_{j=1}^{N} (S_j - 1)\, C_{vi}} \tag{4.41}$$

where N is the total number of solids and the subscript i corresponds to the i^{th} component of the solids mixture.

Thus, with appropriately specified fractions of solids, Equations (4.32) and (4.33) can be used in conjunction with Equation (4.31) to determine an equivalent bed angle β_1'. This angle then allows determination of the slip-point gradient $Y_s^{(2)}$ in Equation (4.29).

To complete the model development and obtain a generalized coordinate plot of slip-point loci similar to that done for the single-solid model, a force balance must be written for the fluid layer above the bed. However, such a balance on the fluid layer is independent of the solids fractions and is given by Equation (3.33). With due regard for two-solid nomenclature, this becomes

$$Y_s^{(2)}[1 - a(\beta_2)] + X_s^{(2)} \frac{\xi \sin \beta_2}{\pi a^2(\beta_2)} = \left(\frac{\sin \beta_2 - \beta_2 \cos \beta_2}{\pi}\right), \tag{4.42}$$

where $$X_s^{(2)} = \frac{j_{os}}{j_p^{(2)}} . \qquad (4.43)$$

Development of this two-solid stratified model is still in progress. Evaluation of the various assumptions used in the derivation remains to be performed. Initial results indicate that the model should be useful in predicting slip-point and limit of deposition for large particle run-of-mine hydrotransport in which rock and coal may exist in a stratified flow.

5.0 EXPERIMENTAL INVESTIGATIONS

In Task 1 it was concluded that physically-based models offer the best basis for future plugging prediction capabilities. For these models to provide accurate plugging predictions, the physical phenomena occurring in the flow must be understood and accurately described. Experimental investigations of two physical processes, sliding friction and interfacial shear, were recommended. Based on the review conducted in Task 1 of this study, the objective of these investigations is to obtain data that may be used to support mechanistic modeling of large particle hydrotransport. The experiments and uncertainty analyses are described in this section. Results obtained for the coefficient of friction experiment are discussed.

5.1 COEFFICIENT OF FRICTION EXPERIMENT

In this experiment, the frictional force occurring between a submerged sliding bed of solids and a pipe wall was studied. Parameter effects of particle size, size distribution, and bed height were sought. Four narrow particle size ranges from $\bar{d}/D = 0.05$ to 0.20 were tested using coal and rock.

To determine a coefficient of friction, a test section was constructed in which a submerged bed of solids was inclined and restrained from sliding by a movable plunger. The angle at which the bed slides *en masse*, δ, and the angle subtended by the bed of solids, β, can be related to the coefficient of friction, μ_s, by the following expression:

$$\tan \delta = 2 \mu_s \left(\frac{\sin \beta - \beta \cos \beta}{\beta - \cos \beta \sin \beta} \right). \tag{5.1}$$

Equation (5.1) represents a force balance along the axis of an inclined pipe and is derived by equating the submerged weight of the bed with the resisting force due to friction when oriented at angle δ.

5.1.1 Experimental Method

Figure 5.1 presents the test section design used in the coefficient of friction experiment. Two 2.1-m long, 0.15-m diameter test sections were

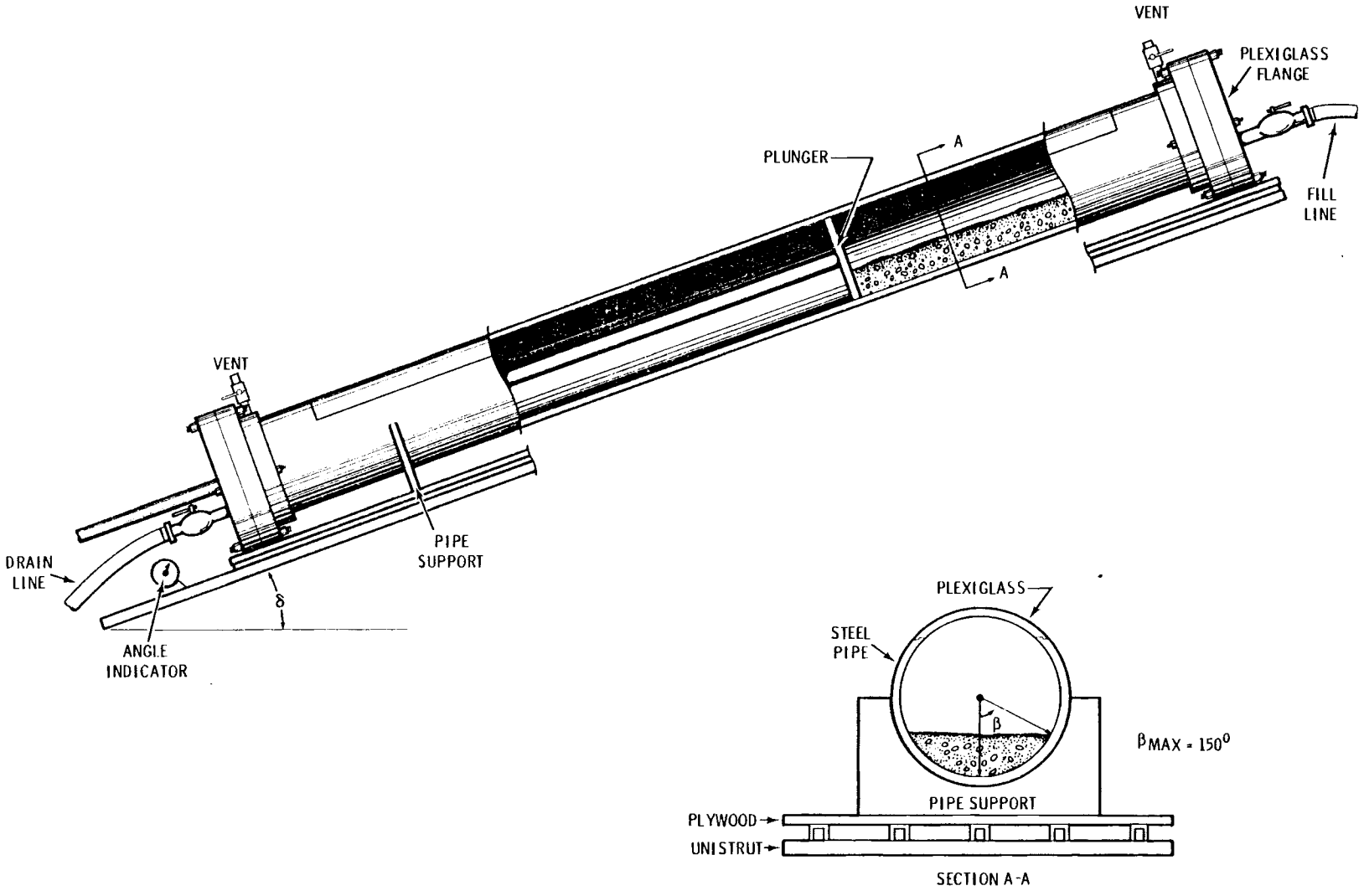

FIGURE 5.1. Test Section for the Coefficient of Friction Experiment

fabricated from a Schedule 40 carbon steel pipe and a plastic PVC pipe. The top one-third portion of each pipe was cut out and replaced with transparent plexiglass sections to facilitate viewing of the sliding solids bed.

A plunger, which allowed water but no solids to pass, was connected to a rod. The rod exited through a flange at the lower end of the test section. Withdrawal of the plunger was controlled by a hand-operated winch. The bed angle, β, was measured by viewing lines of constant β etched on the plunger through a plexiglass flange located at the upper end of the test section. The angle δ was determined from an angle indicator located at the lower end of the test section.

The entire test section was mounted on a plywood and unistrut base and was balanced at its center of mass on a 1.2-m high pivot bar. By adjusting the elevation of the lower end, selected angles of δ between 0 and 45° were obtained.

After the angle of inclination was set, particles with a fixed $\bar{d}/D$ ratio were placed inside the test section. A sufficient quantity of solids was added such that a sliding solids bed approximately 0.6-m long was formed. The entire test section was then filled with water and the plunger inserted. The plunger was slowly withdrawn using the hand operated winch. Within the first meter of travel, an equilibrium sliding bed height was reached, in which frontal falling and bed expansion ceased.

With an equilibrium bed height established, the plunger was further withdrawn and the point at which the solids bed moved en masse was noted. After it was determined that the bed did indeed slide, the equilibrium bed height was obtained by viewing the lines of constant β etched on the plunger. With sliding occurring, the angle of inclination was then lowered, the plunger returned, and the test repeated. After determining the angle δ at which the solids no longer slid, the solids bed was removed and replaced by a second bed of the same $\bar{d}/D$ ratio. Testing was performed for the second bed, providing coefficients of friction values for two different beds at a given $\bar{d}/D$ ratio.

Tests with the PVC pipe were performed to establish a viable testing procedure and to estimate the repeatability of the results. The PVC pipe tests also provide data that represent smooth pipe wall conditions, similar to what might be experienced in a corrosion-free hydrotransport system.

Tests with coal in the steel test section were first carried out with a rusted surface, characteristic of a hydrotransport system in which aeration of the slurry occurs and both erosion-corrosion mechanisms result in the production of very rough surfaces. Following the completion of the rusted surface tests, the inside diameter of the pipe was sandblasted. Results for the PVC, rusted and sandblasted steel test sections are presented in Section 5.1.3.

5.1.2 Data Uncertainty

Initial tests with random-sized rock were performed in the PVC test section to establish a viable testing procedure. During these tests, sliding phenomena were observed and noted. These tests were then repeated to estimate the reproducibility of the results. Repeatability of the sliding angle, δ, was 1° and of the angle, β, was $\pm 10^\circ$. The effect of the uncertainty in β and δ on the uncertainty of μ_s is computed as shown below.

The relationship of β and δ to μ_s given by Equation (5.1) can be rearranged as

$$\mu_s = \frac{\tan\delta}{2\left(\frac{\sin\beta - \beta\cos\beta}{\beta - \cos\beta\sin\beta}\right)} = \frac{\tan\delta}{F(\beta)}. \qquad (5.2)$$

The uncertainty of μ_s in Equation (5.2) can be obtained by taking the logarithm of both sides and differentiating the result, or

$$\frac{d\mu_s}{\mu_s} = \frac{d(\tan\delta)}{\tan\delta} - \frac{d[F(\beta)]}{F(\beta)}. \qquad (5.3)$$

With more than one independent variable affecting the result, simple addition of the uncertainty interval of each variable is not valid. This is because

the uncertainty of each variable can take on either positive or negative values and it is unlikely that all of them will be positive for any one given reading. To account for the positive and negative variations that occur, the net uncertainty in μ_s can be computed as the square root of the sum of the squares (RMS) of the uncertainties of the primary variables. The uncertainty in μ_s is thus

$$\left(\frac{d\mu_s}{\mu_s}\right) = \left[\left(\frac{d(\tan\delta)}{\tan\delta}\right)^2 + \left(\frac{d[F(\beta)]}{F(\beta)}\right)^2\right]^{1/2} . \tag{5.4}$$

Evaluating the uncertainty of the primary variables, δ and β, gives

$$\left(\frac{d(\tan\delta)}{\tan\delta}\right)^2 = \left(\frac{\sec^2\delta}{\tan\delta}\right)^2 (d\delta)^2 = \left(\frac{1}{\sin\delta\ \cos\delta}\right)^2 (d\delta)^2 \tag{5.5}$$

and

$$\left(\frac{d[F(\beta)]}{F(\beta)}\right)^2 = \left(\frac{-2\ \sin\ \beta + \beta\ \sin^2\beta\ \cos\beta + \beta^2\ \sin\beta}{(\beta - \cos\beta\ \sin\beta)\ (\sin\beta - \beta\ \cos\beta)}\right)^2 (d\beta)^2 \tag{5.6}$$

The $d\delta$ and $d\beta$ terms in Equations (5.5) and (5.6) correspond to the $\pm 1^\circ$ and $\pm 10^\circ$ fluctuations in the measurements of δ and β. The uncertainty of β was relatively high because of the jagged nature of the bed surface. A graph of the uncertainty in μ_s as a function of β for various sliding angles, δ, is shown in Figure 5.2. Note that the uncertainty in μ_s increases sharply for angles of δ less than 25° for a fixed bed angle β. The error introduced by the uncertainty in β increases with increasing β until $\beta = 120^\circ$, at which point the error begins to decrease. From Figure 5.2 it can be determined that μ_s is accurate to $\pm 10\%$ for $15^\circ < \delta < 40^\circ$. Sliding angles outside this range were neither anticipated nor measured in this work.

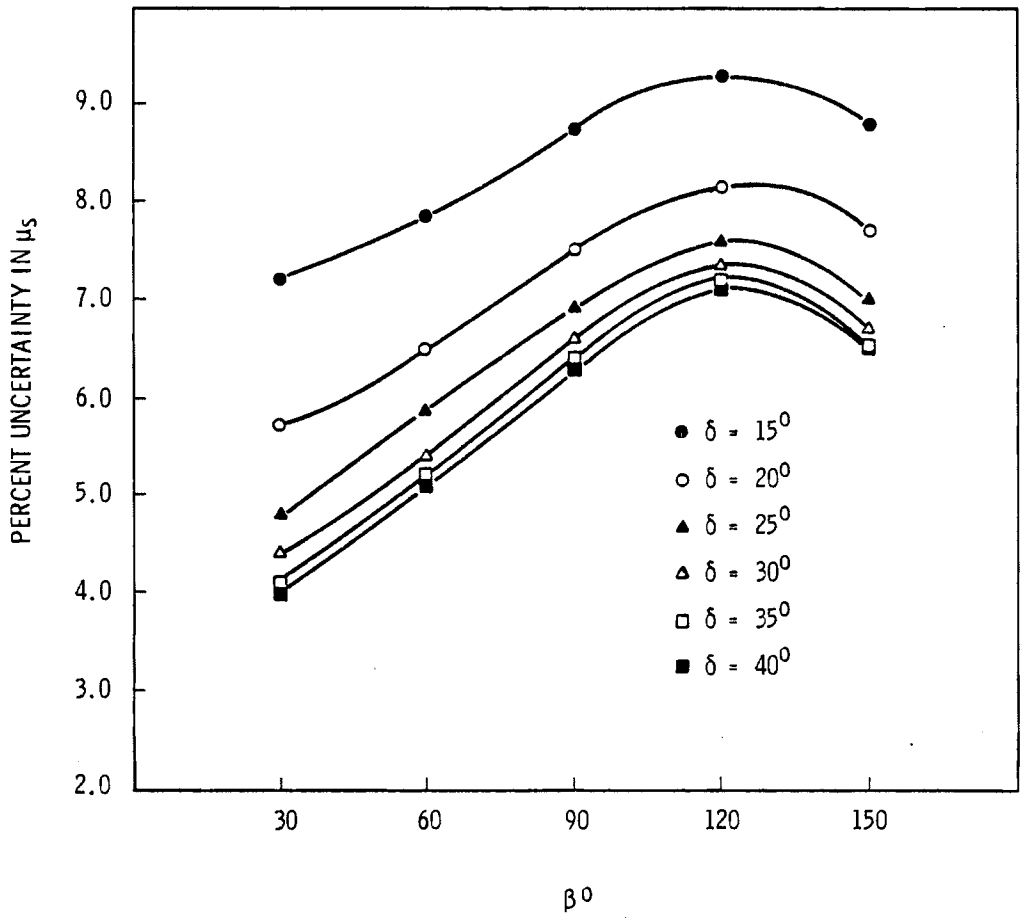

FIGURE 5.2. Uncertainty in μ_S versus β for Various Sliding Angles

5.1.3 Experimental Results and Discussion

The coefficient of friction for a submerged sliding bed of narrow-sized coal on three types of surfaces was measured. Figure 5.3 displays the resulting coefficient of friction values for rusted steel, sandblasted steel, and PVC pipe surfaces as a function of $\bar{d}/D$. These values of μ_s were obtained as a function of β and δ using Equation (5.2).

Test results indicate the coefficient of friction for rusted and sandblasted steel pipe is not a function of particle size. The coefficient of friction for both the rusted and sandblasted surface conditions was found to be 0.5 ±0.05 over the $\bar{d}/D$ ratios examined. Of the two steel surface conditions, the data for the rusted steel pipe were found to exhibit slightly lower coefficient of friction values. This observation may be a consequence of the presence of rust deposits in the valleys between surface roughness peaks, hence reducing the effects of surface imperfections.

Data from the PVC pipe showed a more pronounced effect due to particle size, with μ_s decreasing as $\bar{d}/D$ increases. The coefficient of friction for the PVC pipe was found to be considerably lower than the steel value due to the reduced surface roughness and fewer surface imperfections. The coefficient of friction for the PVC surface was correlated as a linear function of $\bar{d}/D$ as

$$\mu_s = -0.69(\bar{d}/D) + 0.39 \ . \qquad (5.7)$$

The data fit this expression to within ±10%, which is the estimated uncertainty of this experiment.

As indicated by the results shown in Figure 5.3, data for the PVC section clearly show a $\bar{d}/D$ dependence. This effect was not observed for the steel test section. Although there is no conclusive evidence to explain this phenomenon, the increased surface roughness and greater number of surface imperfections in the steel pipe may have tended to eliminate any $\bar{d}/D$ dependence.

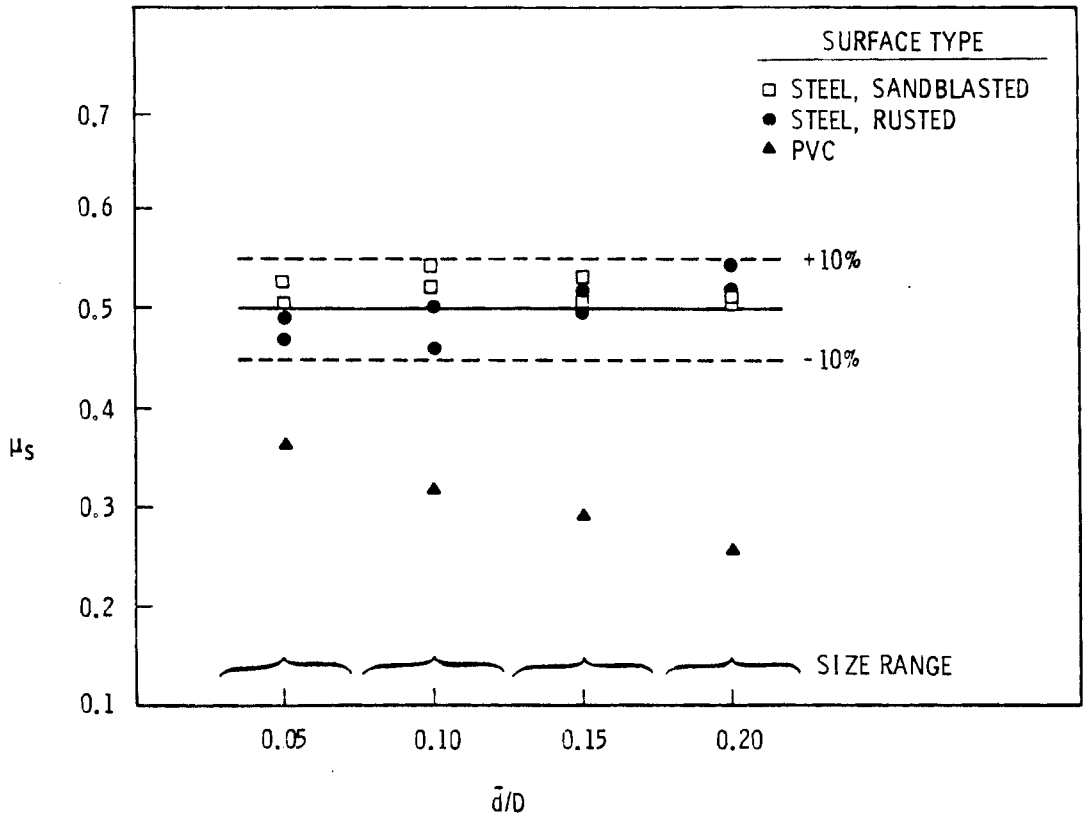

FIGURE 5.3. Coefficient of Friction Results for Coal on Various Surfaces

Tests were also performed with coal in a dry, sandblasted steel pipe. Results over the entire $\bar{d}/D$ range were higher than the wet case by typically 10%, thus indicating a lubricating effect of the fluid layer between the solids and pipe wall.

Figure 5.4 displays the friction coefficient results for crushed rock and coal using the steel and PVC test sections. For both surface types, the resulting coefficient of friction values for crushed rock showed no particle size dependence and were found to be higher than the coal values. The increased coefficient of friction values for the crushed rock can be attributed to the increased specific gravity and the surface roughness of the crushed rock. The results for the PVC test section further support the conclusion that very rough surfaces (for either the pipe or particles) tend to eliminate any particle size dependence.

In summary, results from the sliding bed tests indicate

- the coefficient of friction values for sandblasted and rusted steel pipe are similar and do not show a $\bar{d}/D$ dependence with μ_s being $\sim 0.5 \pm 0.05$
- the coefficient of friction values for PVC pipe exhibit a $\bar{d}/D$ dependence, are approximately 40% lower than the coefficient for steel, and were within ±10% of $\mu_s = -0.69(\bar{d}/D) + 0.39$
- the coefficient of friction values for crushed rock do not demonstrate a $\bar{d}/D$ dependence and are greater than coal values for both the PVC and steel test sections
- the coefficient of friction is less when the solids are submerged in water than when sliding dry.

The results from this experiment can be used as input to the slip-point limit of deposition model developed in Section 3.3.2. The observation that the coefficient of friction for the PVC pipe leads to a lower resistance force is also useful in relation to the work of Baker and Jacobs (1976). They found in wear measurement tests that PVC wear rates were about one-half those in steel pipe for ore transport. Thus, lower resisting force and lower wear

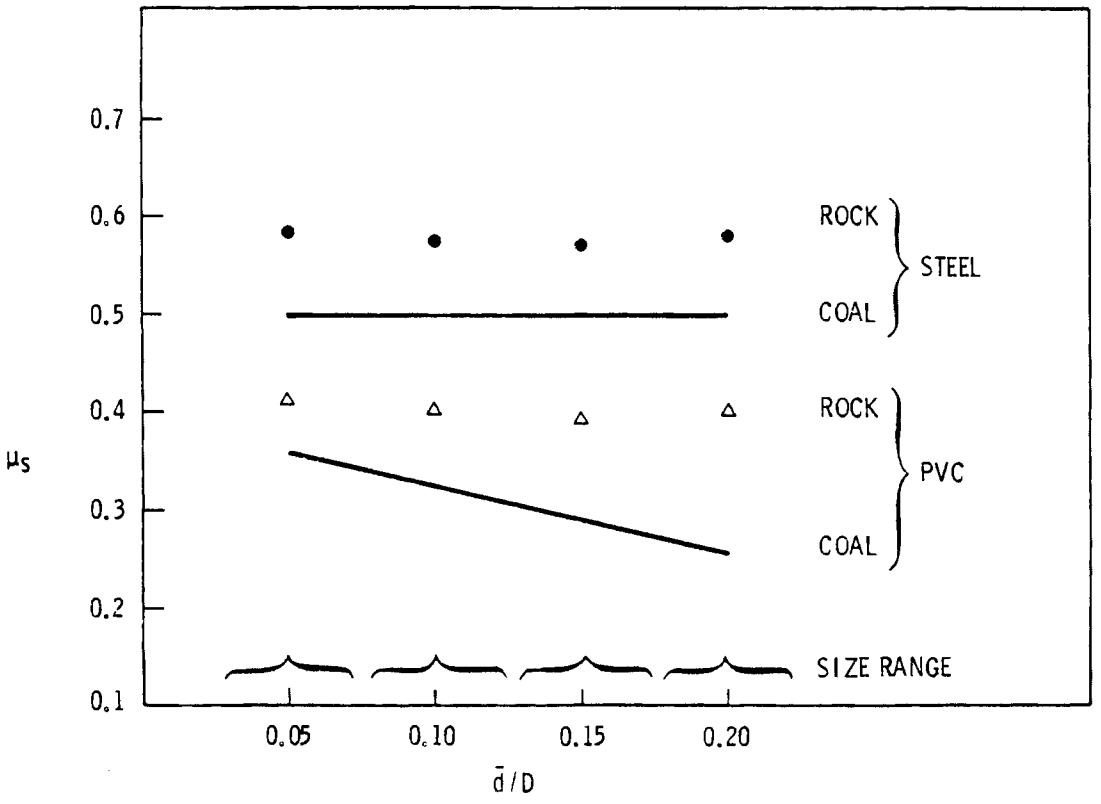

FIGURE 5.4. Coefficient of Friction Results for Coal and Rock on Various Surfaces

rates suggest that use of a smooth PVC pipe would be advantageous in a hydrotransport system if other restraints, such as pressure limitations, can be overcome.

5.2 INTERFACIAL SHEAR EXPERIMENT

With a stationary or sliding bed present in a pipe invert, a shear force created by the velocity difference between the carrier fluid above the bed and the bed itself exists at the bed interface. The interfacial shear caused by this velocity difference acts as a driving force on a solids bed and therefore must be included in any physically based model. In this experiment, the interfacial shear force will be determined through measurement of an interfacial friction factor. The data obtained from these tests will be used either in support of the approach currently used in the single-solid model or as a data base for developing an alternative approach.

The origin of the interfacial shear term in the single-solid model was presented in Section 3.3.2. The experiment intended to perform the measurements necessary to model interfacial shear is currently in the design stage. A description of the experiment, design calculations, and an uncertainty analysis are presented in this section.

5.2.1 Description of Proposed Test Section and Loop

A schematic of the proposed test loop is shown in Figure 5.5. An initial conceptual design of the cross section of the test section is detailed in Figure 5.6. The test section consists of pipe sections with a transparent top for interface viewing. Pressure taps located at equal intervals along the test section allow the bed friction factor, f_i, to be determined. Fluid velocity is determined using a flowmeter upstream of the test section. If necessary, interim storage tanks, screens, and a filtration system are located on the downstream side. Current plans will allow this test section to be incorporated directly with a 1000-gpm process water source. Only minor piping changes and the addition of a downstream filtration system will be necessary.

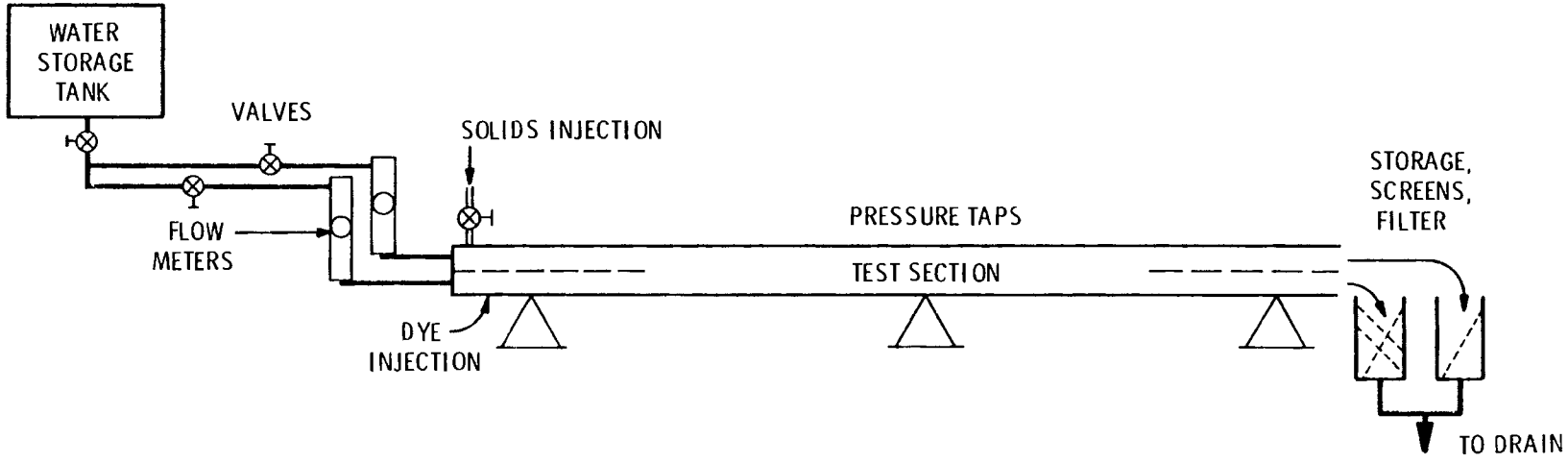

FIGURE 5.5. Proposed Test Loop for the Interfacial Shear Experiment

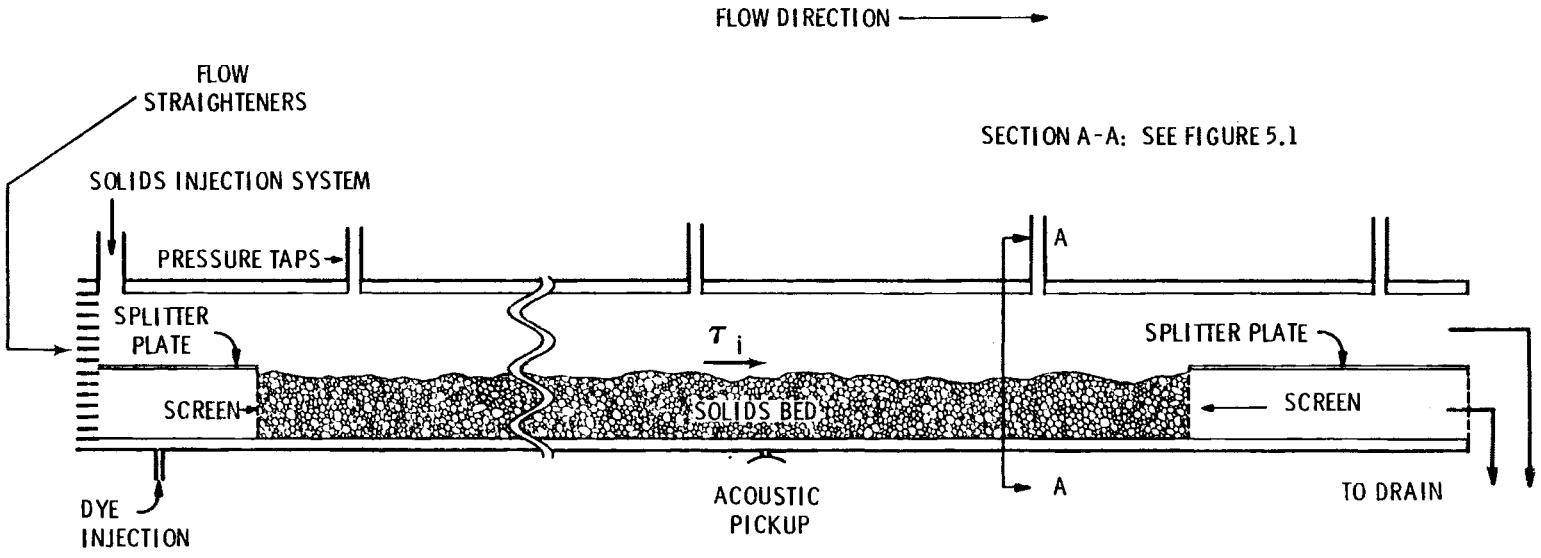

FIGURE 5.6. Proposed Test Section for the Interfacial Shear Experiment

An injection port from a pressurized holding tank or another method of solids injection will allow injection of solids upstream of the test bed. This will be designed to allow investigation of interface phenomena in the limit when solids are stationary next to the wall, but the interface may move. A dye injection system will be used to visualize interlayer fluid mixing and throughbed fluid flow.

One of the main parameters of interest in these experiments will be solids particle size. Thus, several test beds will be used, composed initially of narrow-sized consist and subsequently of wide-sized mixtures. Ultimately, tests with narrow-sized and wide-sized mixtures of materials of different specific gravity will be tested to gain information most applicable to run-of-mine type coal, wherein rock and other debris may exist.

5.2.2 Design Calculations

The interfacial shear, τ_i, produced by a carrier fluid moving at a velocity V_a above a stationary bed can be expressed as

$$\tau_i = f_i \frac{\rho V_a^2}{8} \tag{5.8}$$

where f_i is a Darcy-Weisbach friction factor for the interface and ρ is the carrier fluid density. By knowing f_i as a function of particle size, bed height, and fluid velocity, the absolute value of the interfacial shear stress can be determined. Hence, through proper modeling of f_i, the interfacial shear can be adequately described.

The pressure drop, ΔP, in a pipe length, L, having an equivalent hydraulic inside diameter D_h, and an average velocity V_a, is given by the Darcy-Weisbach equation as

$$\frac{\Delta P}{L} = f \frac{V_a^2}{2gD_h} \tag{5.9}$$

where f is the friction factor for a pipe without a solids bed. This equation expresses the pressure drop due to fluid friction and can be analytically derived through dimensional analysis, with the exception of the friction factor, f. The friction factor can be determined experimentally from a reworking of Equation (5.9) as

$$f = \frac{\Delta P/L}{V_a^2/2gD_h}. \tag{5.10}$$

Thus, the pressure drop per unit length and the fluid velocity above the bed must be measured.

To estimate the change in friction factor with and without a solids bed, assume that flow exists in the upper half of a 0.157-m diameter pipe in which a horizontal plate has been inserted across the diameter ($\beta = 90^\circ$). Furthermore, assume that the fluid velocity is less than that estimated for turbulent suspension of the coal particles ($V_a \simeq 1$ m/sec).

Computation of the friction factor for this semicircular flow section, f_{plate}, can be performed via the Colebrook and White equation. In this equation, the friction factor, f_{plate}, is a function of relative roughness (the ratio of surface roughness, ε, to pipe diameter, D) and Reynolds number, Re, as

$$\frac{1}{\sqrt{f_{plate}}} = -0.86 \ln\left(\frac{\varepsilon/D}{3.7} + \frac{2.51}{Re\sqrt{f_{plate}}}\right). \tag{5.11}$$

Since the flow channel is noncircular, computation of the Reynolds number and relative roughness for use in the Colebrook and White equation must be made using an equivalent hydraulic diameter, D_h:

$$D_h = \frac{4(\text{Flow Area})}{\text{Wetted Perimeter}} = \frac{\pi D}{\pi + 2}. \tag{5.12}$$

Using typical values, the Reynolds number becomes

$$Re = \frac{D_h V_a}{\nu} \tag{5.13}$$

$$= \frac{\left[\frac{\pi(0.157\ m)}{\pi + 2}\right]\left(\frac{1\ m}{sec}\right)}{\left(0.98 \times 10^{-6}\ \frac{m^2}{sec}\right)} = 86,500 \quad . \tag{5.14}$$

A typical value for the surface roughness of commercial steel pipe is 4.6×10^{-5} m. This leads to a relative roughness of

$$\frac{\varepsilon}{D_h} = \frac{(4.6 \times 10^{-5}\ m)}{\frac{\pi\ (0.157\ m)}{\pi + 2}} = 4.80 \times 10^{-4} \quad . \tag{5.15}$$

Substitution of the relative roughness and Reynolds number into Equation (5.11) yields a friction factor for a semicircular flow section, $f_{plate} = 0.021$.

To simulate the presence of a fixed bed, assume that uniform-sized solid particles with a particle-to-pipe diameter ratio ($\bar{d}/D_h$) of 0.085 have been fixed onto the steel plate. With β and the flow velocity, V_a, fixed, the flow area and, subsequently, the Reynolds number, remain the same. One must note, however, that the relative roughness of the plate surface is greatly increased by the presence of solid particles.

For calculations in this composite flow section, it is assumed that the total friction factor with the presence of a bed, f_{bed}, is composed of f_i, an interfacial friction factor due to the surface roughness of the fixed particles on the plate, and f_{wall}, the friction factor due to the surface roughness of the wall. It is further assumed that the effect of f_i can be superimposed on f_{wall} if the difference in surface areas of the wall and plate are accounted for. To estimate the contribution of f_i and f_{wall} to f_{bed}, area ratios are used:

$$f_{bed} = f_i \left(\frac{A_{plate}}{A_{wall} + A_{plate}} \right) + f_{wall} \left(\frac{A_{wall}}{A_{wall} + A_{plate}} \right) \qquad (5.17)$$

where A_{plate} and A_{wall} are the areas of the plate and wall, respectively.

The value of f_{wall} is equivalent to the value of f_{plate} presented earlier, because the Reynolds number and wall surface roughness have remained unchanged. The friction factor at the interface, f_i, also depends upon these two parameters. However, with particles fixed onto the plate, particle diameter, rather than surface roughness, becomes important.

An estimate of f_i can therefore be made by replacing surface roughness, ε, with particle diameter, d, in the Colebrook and White equation. Substitution of particle diameter in the Colebrook and White equation [Equation (5.11)] results in

$$\frac{1}{\sqrt{f_i}} = -0.86 \ln \left(\frac{d/D}{3.7} + \frac{2.51}{Re \sqrt{f_i}} \right) . \qquad (5.18)$$

Using the previously computed Reynolds number and the particle-to-hydraulic diameter ratio in Equation (5.18) results in a value for f_i of 0.094. The friction factor for a bed of solids, f_{bed}, can now be evaluated by substitution of f_i, f_{wall} and the proper area ratios into Equations (5.17). This yields a value for f_{bed} of 0.047.

The percentage change in the friction factor with and without a bed of solids is computed as

$$\% \text{ change in } f = \left[\frac{f_{bed} - f_{steel}}{f_{steel}} \right] \times 100 \qquad (5.19)$$

$$= \left[\frac{0.047 - 0.021}{0.021} \right] \times 100 = 125\% . \qquad (5.20)$$

From these preliminary computations, a 125% increase in the pressure drop due to the presence of a solids bed surface may be anticipated.

The difference of $f_{bed} - f_{plate}$ is due solely to the presence of the solids bed interface. This difference, an effective interfacial friction factor, $f_{i,eff}$, is the parameter this experiment intends to measure. The interfacial shear force can be computed from Equation (5.8) using the measured friction factor as

$$\tau_i = f_{i,eff} \rho \frac{V_a^2}{8} \tag{5.21}$$

where

$$f_{i,eff} = f_{bed} - f_{plate} \tag{5.22}$$

Substitution of the proper values into Equation (5.21) results in an interfacial shear force of

$$\tau_i = \frac{(0.026)\ (1000\ kgm/m^3)\ (1\ m/sec)^2}{(8)} \tag{5.23}$$

$$= 3.25\ N/m^2.$$

Results from these preliminary design calculations indicate that the interfacial shear force is a small, but measurable, quantity. Its value can be determined indirectly from pressure drop measurements made with and without a solids bed interface at a constant velocity and hydraulic diameter.

5.2.3 Uncertainty Analysis

The effective interfacial friction factor, $f_{i,eff}$, is a small number computed as the difference of two relatively small numbers. Thus, $f_{i,eff}$ and subsequently, τ_i, are potentially subject to considerable uncertainty.

For this error analysis, it will be assumed that all properties are known with negligible uncertainty, but that the flow velocities and pressure drops are subject to uncertainties that can be estimated. The net uncertainty in $f_{i,eff}$ will be computed as the RMS of the uncertainties in the primary variables.

The uncertainty in τ_i can be obtained by taking the logarithm of Equation (5.8),

$$\ln \tau_i = \ln f_{i,eff} + \ln \rho + 2\ln V_a - \ln 8, \tag{5.24}$$

differentiating the result, and squaring the terms to give

$$\frac{d\tau_i}{\tau_i} = \left[\left(\frac{df_{i,eff}}{f_{i,eff}}\right)^2 + 4\left(\frac{dV_a}{V_a}\right)^2\right]^{1/2}. \tag{5.25}$$

The uncertainty in $f_{i,eff}$ can be represented using

$$f_{i,eff} = f_{bed} - f_{plate} \tag{5.26}$$

$$= \frac{\left[(\Delta P)_{bed} - (\Delta P)_{plate}\right]/L}{V_a^2/2gD_h} \tag{5.27}$$

where $(\Delta P)_{bed}$ and $(\Delta P)_{plate}$ are the pressure drops for a pipe with a solids bed and a pipe with a plate, respectively. Taking the logarithm of Equation (5.26) yields

$$\ln(f_{i,eff}) = \ln[(\Delta P)_{bed} - (\Delta P)_{plate}]$$

$$+ \ln 2 + \ln g + \ln D_h - 2\ln V_a - \ln L \tag{5.28}$$

Differentiating Equation (5.27) and squaring the terms results in the uncertainty in $f_{i,eff}$ of

$$\left(\frac{df_{i,eff}}{f_{i,eff}}\right)^2 = 2\left(\frac{d(\Delta P)}{(\Delta P)_{bed} - (\Delta P)_{plate}}\right)^2 + \left(\frac{dD_h}{D_h}\right)^2$$

$$+ 4\left(\frac{dV_a}{V_a}\right)^2 + \left(\frac{dL}{L}\right)^2 \qquad (5.29)$$

where it is assumed that the error in pressure drop measurement for the test section with and without a solids bed is the same, $d(\Delta P)_{plate} = d(\Delta P)_{bed} = d\Delta P$.

Combining Equation (5.25) with Equation (5.29) results in the total uncertainty for τ_i,

$$\frac{d\tau_i}{\tau_i} = \left[\left(\frac{d\Delta P}{(\Delta P)_{bed} - (\Delta P)_{plate}}\right)^2 + 8\left(\frac{dV_a}{V_a}\right)^2 + \left(\frac{dD_h}{D_h}\right)^2 + \left(\frac{dL}{L}\right)^2\right]^{1/2} . \qquad (5.30)$$

Using the design calculation case results in

$$\left(\frac{dL}{L}\right) = \frac{0.01\ m}{30\ m} = 0.033\%, \qquad (5.31)$$

$$\left(\frac{dD_h}{D_h}\right) = \frac{0.01\ m}{0.096\ m} = 10.4\%, \qquad (5.32)$$

and

$$\left(\frac{dV_a}{V_a}\right) = \frac{0.05\ m/sec}{1.0\ m/sec} = 5.0\% \ . \qquad (5.33)$$

Computation of the pressure losses for the uncertainty in $f_{i,eff}$ can be made with f_{bed}, f_{plate}, and Equation (5.9),

$$(\Delta P_{bed} - \Delta P_{plate}) = (f_{bed} - f_{plate}) \frac{LV_a^2}{2gD_h}$$

$$= \frac{(0.47 - 0.21)\ (30\ m)(1\ m/sec)^2}{2\ (9.81\ m/sec^2)\ (0.096\ m)}$$

$$= 0.41\ m_{H_2O} \ . \qquad (5.34)$$

With an estimated pressure measurement error of 0.01 m_{H_2O}, the relative error becomes

$$\left(\frac{d\Delta P}{(\Delta P)_{bed} - (\Delta P)_{plate}} \right) = \frac{0.01}{0.41} = 2.5\% \ . \qquad (5.35)$$

Substituting Equations (5.31) through (3.34) into Equation (5.30) gives an uncertainty for $d\tau_i/\tau_i$ of 18%.

This uncertainty estimate is based on preliminary design data. As more details for the experiment become available, the analysis will be updated. In light of uncertainties associated with the current method of determining interfacial shear, ±18% is an acceptable limit.

REFERENCES

Alger, G. L., and D. B. Simons. 1968. "Fall Velocity of Irregular Shaped Particles." Journal of the Hydraulics Division, ASCE, HY3:721-737.

Baker, P. J., and B. E. A. Jacobs. 1976. "The Measurement of Wear in Pumps and Pipelines." In HYDROTRANSPORT 4, Paper J1, BHRA Fluid Engineering, Cranfield, England.

Carleton, A. J., et al. 1978. "Hydraulic Transport of Large Particles Using Conventional and High Concentration Conveying." In HYDROTRANSPORT 5, Paper D2, BHRA Fluid Engineering, Cranfield, England.

Faddick, R. R. 1974. Properties of Coal-Water Slurries. OFR 53-76, U.S. Department of the Interior, Bureau of Mines, Washington, D.C.

Ferrini, F., et al. 1978. "Shear Viscosity of Settling Suspensions." Presented to the Third International Technical Conference on Slurry Transportation, Slurry Transport Association, Las Vegas, Nevada.

Funk, E. D., M. D. Baker, and D. W. Hunter. 1978. "Pilot Experiences with Run of Mine Coal Injection and Pipelining." In HYDROTRANSPORT 5, Paper F3, BHRA Fluid Engineering, Cranfield, England.

Gandhi, R. L., and T. C. Aude. 1978. "Slurry Pipeline Design--Special Considerations." In HYDROTRANSPORT 5, Paper J1, BHRA Fluid Engineering, Cranfield, England.

Haas, D. B., W. H. W. Husband, and C. A. Shook. 1978. "The Development of Hydraulic Transport of Large Sized Coal in Canada--Phase I." In HYDROTRANSPORT 5, Paper H1, BHRA Fluid Engineering, Cranfield, England.

Hisamitsu, N., Y. Shoji, and S. Kosugi. 1978. "Effect of Added Fine Particles on Flow Properties of Settling Slurries." In HYDROTRANSPORT 5, Paper D3, BHRA Fluid Engineering, Cranfield, England.

Judge, D. G. 1979. _____. Master's Thesis, Queens University, Kingston, Ontario, Canada.

Kao, D. T. 1976. "On Mechanism of Slurry Flow Re-initiation." In HYDROSTRANSPORT 4, contributed paper, BHRA Fluid Engineering, Cranfield, England.

Kazanskij, I. 1976. "Behaviour of Extremely Coarse Particles in Pipe Flow." In HYDROTRANSPORT 4, Paper A2, BHRA Fluid Engineering, Cranfield, England.

Lazarus, H. J., and I. D. Nielson. 1978. "A Generalized Correlation for Friction Head Losses of Settling Mixtures in Horizontal Smooth Pipelines." In HYDROTRANSPORT 5, Paper B1, BHRA Fluid Engineering, Cranfield, England.

Link, J. M., R. R. Faddick, G. A. Pouska, and J. J. Gusek. 1977. Hydraulic Transportation of Oil Shale. CSMRI Report C51149, Colorado School of Mines Research Institute, Golden, Colorado.

Masliyah, J. H., and C. A. Shook. 1978. "Two-Phase Laminar Zero Net Flow in a Circular Inclined Pipe." Canadian J. of Chem. Engr. 56:165.

Newitt, D. M., M. Abbott, J. F. Richardson, and R. B. Turtle. 1955. "Hydraulic Conveying of Solids in Horizontal Pipes." Trans. Inst. Chem. Engineers. 33(2).

Pouska, G. A., and J. M. Link. 1978. "Investigation of Head Losses in Coarse Oil Shale Slurries." In HYDROTRANSPORT 5, Paper H2, BHRA Fluid Engineering, Cranfield, England.

Sakamoto, M., M. Mase, Y. Nagawa, K. Uchida, and Y. Kamino. 1978. "A Hydraulic Transport Study of Coarse Materials Including Fine Particles with Hydrohoist." In HYDROTRANSPORT 5, Paper D6, BHRA Fluid Engineering, Cranfield, England.

Šašić, M., and P. Marjanović. 1978. "On the Methods of Calculation of Hydraulic Transport and Their Reliability in Practice." In HYDROTRANSPORT 5, Paper A5, BHRA Fluid Engineering, Cranfield, England.

Sauerman, H. B. 1978. "Hydraulic Transportation in a Segmented Pipe." In HYDROTRANSPORT 5, Paper A4, BHRA Fluid Engineering, Cranfield, England.

Scheidegger, A. E. 1960. The Physics of Flow Through Porous Media. MacMillan Co., New York, New York.

Scott, S. A., and T. R. Young. 1972. "Hydraulic Transportation." Surface Mining. Article 9.5, p. 622.

Shook, C. A., D. B. Haas, W. H. W. Husband, A. D. Richardson, and L. G. Smith. 1976. "A Vertical Tube Viscometer for Suspensions Containing Coarse Particles." In HYDROTRANSPORT 4, Paper F4, BHRA Fluid Engineering, Cranfield, England.

Televantos, Y. 1977. The Flow Mechanism of Hydraulic Conveying at High Solids Concentration. Ph.D. Dissertation, Imperial College, London, England.

Turian, R. M., and T. F. Yuan. 1977. "Flow of Slurries in Pipelines." AICHE. 23.

Vocaldo, J. J. 1976. "Role of Some Parameters and Effective Variables in Turbulent Slurry Flow." In HYDROTRANSPORT 4, Paper D4, BHRA Fluid Engineering, Cranfield, England.

Wang, R. C. and J. J. Seman. 1973. Solid-Liquid Flow in Noncircular Pipes. RI-7725, U.S. Department of the Interior, Bureau of Mines, Washington, D.C.

Wiedenroth, W. 1978. "Experimental Work on the Transportation of Solid-Liquid Mixtures Through Pipelines and Centrifugal Pumps." In HYDROTRANSPORT 5, Paper A2, BHRA Fluid Engineering, Cranfield, England.

Wiedenroth, W., and M. Kirchner. 1972. "A Summary and Comparison of Known Calculations of Critical Velocity of Solid-Water Mixtures and Some Aspects of the Optimization of Pipelines." In HYDROTRANSPORT 2, Paper E1, BHRA Fluid Engineering, Cranfield, England.

Wilson, K. C. 1972. "A Formula for the Velocity Required to Initiate Particle Suspension in Pipeline Flow." In HYDROTRANSPORT 2, Paper E2, BHRA Fluid Engineering, Cranfield, England.

Wilson, K. C. 1976. "A Unified Physically-Based Analysis of Solid-Liquid Pipeline Flow." In HYDROTRANSPORT 4, Paper A1, BHRA Fluid Engineering, Cranfield, England.

Wilson, K. C. 1974. "Coordinates for the Limit of Deposition in Pipeline Flow." In HYDROTRANSPORT 3, Paper E1, BHRA Fluid Engineering, Cranfield, England.

Wilson, K. C., and A. Brebner. 1971. "On Two-Phase Pressurized and Unpressurized Flow: Behaviour Near Deposition Points." In Advances in Solid-Liquid Flow in Pipes and Its Applications, ed. I. Zandi. Pergamon Press, Elmsford, New York.

Wilson, K. C., and D. G. Judge. 1978. "Analytically-Based Nomographic Charts for Sand-Water Flow." In HYDROTRANSPORT 5, Paper A1, BHRA Fluid Engineering, Cranfield, England.

Wilson, K. C., M. Streat, and R. A. Bantin. 1972. "Slip-Model Correlation of Dense Two-Phase Flow." In HYDROTRANSPORT 2, Paper B1, BHRA Fluid Engineering, Cranfield, England.

Wilson, K. C., and W. E. Watt. 1974. "Influence of Particle Diameter on the Turbulent Support of Solids in Pipeline Flow." In HYDROTRANSPORT 3, Paper D1, BHRA Fluid Engineering, Cranfield, England.

Wong, A. K. C., and T. S. Liu. 1972. A Numerical Model for the Study of Particle Interactions in Relation to Hydraulic Transport. OFR 5-73, U.S. Department of the Interior, Bureau of Mines, Washington, D.C.

Worster, R. C., and D. F. Denny. 1955. "Hydraulic Transport of Solid Materials in Pipes." Inst. Mech. Engr. Proc. 69:563-586.

DISTRIBUTION

No. of Copies

OFFSITE

A. A. Churm
DOE Patent Division
9800 S. Cass Avenue
Argonne, IL 60439

10 A. J. Miscoe
U.S. DOE
Pittsburgh Mining Technology Center
4800 Forbes Avenue
Pittsburgh, PA 15213

D. Uthus
U.S. DOE
Division of Fossil Fuel Extraction
Mail Drop D-107
Washington, DC 20545

R. C. Wang
4800 Forbes Avenue
Pittsburgh, PA 15213

27 DOE Technical Information Center

R. R. Faddick
Colorado School of Mines
Golden, CO 80401

ONSITE

DOE Richland Operations Office

H. E. Ransom

29 Pacific Northwest Laboratory

J. M. Creer
A. J. Currie
W. I. Enderlin
L. L. Eyler (5)

No. of Copies

W. W. Laity (2)
N. J. Lombardo (10)
J. W. Shupe
A. M. Sutey
Technical Information (5)
Publishing Coordination Ei (2)